



**NTNU – Trondheim**  
Norwegian University of  
Science and Technology

# Design of Composite Tubes Applied in Well Intervention

Komposittrør for anvendelse i oljebrønner

**Dan Eirik Voldnes**

Master of Science in Mechanical Engineering

Submission date: July 2012

Supervisor: Nils Petter Vedvik, IPM

Norwegian University of Science and Technology  
Department of Engineering Design and Materials



THE NORWEGIAN UNIVERSITY  
OF SCIENCE AND TECHNOLOGY  
DEPARTMENT OF ENGINEERING DESIGN  
AND MATERIALS

**MASTER THESIS SPRING 2012  
FOR  
STUD.TECHN. DAN EIRIK VOLDNES**

**DESIGN OF COMPOSITE TUBES APPLIED IN WELL INTERVENTION  
Komposittrør for anvendelse i oljebrønner**


Advanced composite materials and structures having low weight, high stiffness, high strength, and chemical resistance can be utilized in order to obtain low weight high capacity tubes for well intervention. Such tubes, when deployed in oil and gas wells with high temperature, high pressure and aggressive environment, must be designed with respect of both external pressure capacity, longitudinal stiffness and strength capacity, buckling capacity, and specific thermal and chemical resistance.

In the current master thesis work, general and particular aspects of such tubes shall be studied. Relevant tasks are: review of state-of-art, requirements, development of concepts, numerical analysis, production of prototypes by filament winding, and testing.

The thesis should include the signed problem text, and be written as a research report with summary both in English and Norwegian, conclusion, literature references, table of contents, etc. During preparation of the text, the candidate should make efforts to create a well arranged and well written report. To ease the evaluation of the thesis, it is important to cross-reference text, tables and figures. For evaluation of the work a thorough discussion of results is appreciated.

Three weeks after start of the thesis work, an A3 sheet illustrating the work is to be handed in. A template for this presentation is available on the IPM's web site under the menu "Undervisning". This sheet should be updated when the Master's thesis is submitted.

The thesis shall be submitted electronically via DAIM, NTNU's system for Digital Archiving and Submission of Master's thesis.

  
Torgeir Welo  
Head of Division

  
Nils Petter Vedvik  
Professor/Supervisor



## **Acknowledgements**

First and foremost I want to thank my parents for all help and support through all my years in school.

Secondly I would like to thank everyone providing me with valuable input at the Department of Engineering Design and Materials.

Thanks to Anton Antonrulrajah for good discussions and help with completing my experimental testing.

Last but not least I want to express my sincere gratitude to Associate Professor Nils Petter Vedvik which has provided me with guidance and resources throughout my whole senior year.

*Stud.techn. Dan Eirik Voldnes, Trondheim, July 2012.*

## **Abstract**

Carbon composite materials and structures have low weight, high stiffness, high strength and chemical resistance. Throughout this master thesis a feasibility study to utilize carbon composites in tubes, designed to withstand high pressures, is undertaken both analytically and experimentally.

The tube is meant to be used for well intervention, replacing the current solid carbon rod. In such operations is low weight, in addition to above mentioned properties, a critical factor for long reach. To extend the reach of the equipment the submerged weight of such a tube must be as low as possible.

To enable a tube to withstand the high pressures, which can reach more than 1000bar, a thick walled tube is the only alternative to decrease the submerged weight compared to a solid rod. Work and literature on thick walled composite tubes with inner diameter to thickness ratios as low as 2 is minimal, if not absent.

A two layered laminate structure was chosen for the tube. The inner layer existing of hoop winded fibers and the outer layer of longitudinal UD fibers. Such a layup will give both high radial strength and axial stiffness.

Throughout the analysis it was found that the cause of failure would be instability. This conclusion was drawn as instability would occur before any of the chosen failure criterions were fulfilled. This implies that the strength of the material is utilized maximally.

The experimental results had good coherency with the analytical results. Results from physical tests had a large scatter, but this was predicted as a result of a manual production process leading to uneven distribution of fibers and medium to large voids.

Several parameters, both regarding load cases and necessary material properties, for the given requirements of the tube have not been assessed. However, results from conducted analytical and experimental work shows that thick walled composite tubes are able to withstand the given loading conditions, together with keeping the submerged weight sufficiently low.

Future work based on the results in this thesis should include test results with statistical significance, analyses on the more complex load cases, optimal laminate design and identifying a suitable matrix material which can withstand the necessary temperature requirement.

## Sammendrag

Karbonfiber kompositter og strukturer har lav vekt, høy stivhet, høy styrke og kjemisk resistens. I arbeidet med denne masteroppgaven er det gjennomført både analytisk og eksperimentelt arbeid i en mulighetsanalyse for bruk av karbonfiberkompositt i rør laget for å motstå høye eksterne trykk.

Dette røret er tenkt brukt i brønn intervensjons operasjoner, som erstatning for dagens solide karbonstav. I slike operasjoner er den lave vekten sammen med de andre nevnte egenskapene en kritisk faktor for å oppnå lang rekkevidde. For å utvide rekkevidden til det eksisterende utstyret må vekten når nedsenket i vann være så lav som mulig.

For å motstå det høye trykket i en brønn, som kan overgå 1000bar, er et tykkvegget rør det eneste alternativet for å både senke vekten og opprettholde nødvendig styrke. Tidligere arbeider og litteratur om komposittrør med indre diameter til tykkelse rate så lav som 2 er minimal, om ikke fraværende.

En to lags laminat struktur ble valgt for røret. Det indre laget er fiber viklet sirkulært (hoop), og det ytterste laget er langsgående fiber (longitudinal). En slik opplegging gir både høy radiell styrke og aksiell stivhet.

I analysene ble det funnet at årsaken til brudd er instabilitet. Denne konklusjonen ble dratt fordi instabiliteten opptrådte før noen av de valgte feilkriteriene var oppfylt. Dette impliserer at styrken i komposittet er utnyttet maksimalt.

De eksperimentelle resultatene hadde god overenstemmelse med de analytiske. Det var stor variasjon, men dette var forventet på grunn av den manuelle produksjonsmetoden som gav rom for ujevn distribusjon av fiber og middels til store porer.

Flere parameter, både for nødvendige materialegenskaper og lasttilfeller, har ikke blitt vurdert. Basert på resultatene i denne oppgaven er det ingen grunn til å dra noen annen konklusjon enn at det er mulig å designe karbonkompositt rør som klarer å motstå de gitte lastene, samtidig som nedsenket vekt minimeres.

Fremtidig arbeid bør inkludere eksperimentelle tester med statistisk signifikans, analyser som omfatter de mer komplekse lasttilfellene, optimalisering av laminatdesignet og identifisering av matriks materiale som kan oppfylle temperaturkravet.

# Contents

1	Introduction.....	1
1.1	Requirement specification.....	2
1.1.1	Load cases.....	2
1.2	Material properties.....	3
1.3	Weight .....	4
1.4	Layups.....	5
1.5	Failure Criteria.....	6
1.6	Bending Radius .....	7
1.7	Longitudinal- and bending- stiffness .....	10
2	Numerical modeling .....	12
2.1	Axisymmetric model .....	12
2.1.1	Mesh .....	12
2.1.2	Loads and boundary conditions.....	13
2.2	3D models.....	13
2.2.1	Linear perturbation model & mesh .....	14
2.2.2	RIKS model & mesh.....	15
2.2.3	Loads and boundary conditions in buckling models.....	15
3	Numerical results.....	16
3.1	Axisymmetric Model.....	16
3.1.1	Relations between physical features and stress .....	19
3.2	Linear perturbation buckling model .....	19
3.2.1	Choosing specimen dimensions.....	20
3.3	RIKS Buckling Model .....	21
3.3.1	Analysis of tube with specimen dimensions .....	22
3.3.2	Analysis of 22mm tube .....	26
3.4	Scaling.....	29
4	Experimental .....	30
4.1	Production of specimens .....	30
4.1.1	Production of longitudinal fiber layer .....	30



4.1.2	Completing specimen .....	31
4.1.3	Estimated elastic properties of specimens .....	32
4.2	Test procedure .....	36
4.3	Test results .....	36
5	Discussion .....	40
5.1	Future work .....	41
6	Conclusion .....	42
7	References .....	43
	Appendix 1 .....	44
	Appendix 2 .....	45
	Appendix 3 .....	46
	Appendix 4 .....	48
	Appendix 5 .....	51

## Table of figures

Figure 1 - The different load cases the tube undertakes. The numbers represent the different load cases described above. ....	3
Figure 2 – Relation between inner and outer diameter of the tube to achieve a satisfactory submerged weight. The red line represents an infinite thin tube.....	4
Figure 3 – The two different layup models. ....	5
Figure 4 - Pucks IFF criterion (Analysis of Failure in Fiber Polymer Laminates, 2008 [6]).	7
Figure 5 – Model for minimum bending radius .....	8
Figure 6 - Meshed axisymmetric model.....	13
Figure 7 - Loads and boundary conditions on axisymmetric model .....	13
Figure 8 - Buckle models mesh .....	14
Figure 9 - Introduction of geometric imperfection in RIKS model. ....	15
Figure 10 - Loads and boundary conditions on buckling models.....	16
Figure 11 - Maximum fiber stresses predicted for each layer as a function of outer diameter, subjected to a compressive force of 50kN (in addition to the outside pressure). ....	17
Figure 12 - Transversal stresses through thickness in tubes with a submerged weight of 0 g/m and equal thickness of hoop and longitudinal fibers, undertaking 50kN tensile force. ....	18
Figure 13 - Transversal stresses through thickness in tubes with a submerged weight of 0 g/m and equal thickness of hoop and longitudinal fibers, undertaking 50kN in compressive force.....	18
Figure 14 - General behavior of the transversal stresses through the thickness. The green lines represent possible states of stress found in the analyses. ....	19
Figure 15 - Pressure validation shown to the left and the two locations for extraction of stress data shown to the right. ....	22
Figure 16 - Fiber stresses, development with increasing pressure, D=16mm, Location 1. Compressive fiber failure predicted at about 75MPa pressure. Instability for inner part of hoop ply occurs at about 50MPa pressure. ....	24
Figure 17 - Fiber stresses, development with increasing pressure, D=16mm, Location 2. Compressive fiber failure predicted at about 65MPa pressure, instability is predicted at about 60MPa pressure.....	24
Figure 18 - Transverse stresses, development with increasing pressure, D=16mm, Location 1. Instability occurs well before Puck criterion predicts failure and predicted to first happen at about 50MPa pressure. ....	25
Figure 19 - Transverse stresses, development with increasing pressure, D=16mm, Location 2. Instability occurs well before Puck criterion predicts failure and predicted to first happen at about 50MPa pressure. ....	25

Figure 20 - Fiber stresses development with increasing pressure, D=22mm, Location 1. No instability before compressive FF occurs (maybe with exception of inner part of hoop ply). Failure predicted at about 180MPa pressure. ....	27
Figure 21 - Fiber stresses development with increasing pressure, D=22mm, Location 2. No instability before FF criterion predicts failure. Failure predicted at approximately 190 MPa pressure. ....	27
Figure 22 - Transverse stresses, development with increasing pressure, D=22mm, Location 1. Instability will occur at about 420MPa pressure, well before failure predicted by Puck criterion. ....	28
Figure 23 - Transverse stresses, development with increasing pressure, D=22mm, Location 2. Instability will occur at about 530MPa pressure, somewhat before predicted failure by Puck criterion. ....	28
Figure 24 – The moulds used for specimen production using approach 2. The holes in the mold facilitate escaping of superfluous resin. ....	31
Figure 25 - Finished specimen with end caps. Silicon is not added on surface yet.....	32
Figure 26 - End cap dimensions (all dimensions in [mm]).....	32
Figure 27 – Microscopy of specimen nr8, zooming in on the hoop fibers (enhancement is indicated in top left corner of each image). This is the original images before rendering. The large crack between the hoop and longitudinal layer in the top left image is believed to be a result of the machining process. ....	33
Figure 28 – Rendered image of hoop fiber layer in specimen nr8, with 500x enhancement. The volume fraction calculated is considered to be somewhat conservative due to the dark edges. Estimated volume fraction: 0,526. ....	34
Figure 29 – Rendered image of hoop fiber layer in specimen nr8, with 500x enhancement. The volume fraction calculated is considered to be somewhat high as space between fibers from parts of picture is quite bright. Estimated volume fraction: 0,596. ....	34
Figure 30 – Rendered image of hoop fiber layer in specimen nr2, with 200x enhancement. Estimated volume fraction: 0,527.....	35
Figure 31 – Recorded pressure vs. time during testing for all specimens. The large decrease in pressure shown for some specimens represents the depressurization of the pressure chamber. ....	36
Figure 32 – Relations between critical pressure and inner diameter to thickness ratio for different length to inner diameter ratios. Hoop to longitudinal stress ratio is 2. (Failure of composite cylinders under combined external pressure and axial loading, 1992 [5])	37
Figure 33 - Specimen 2 after failure. Critical pressure = 91MPa. ....	38
Figure 34 - Specimen 3 after failure. Critical pressure = 105MPa. ....	38
Figure 35 - Specimen 4 after failure. Critical pressure = 70MPa.....	38
Figure 36 - Specimen 6 after failure. Critical pressure = 53MPa.....	39
Figure 37 - Specimen 8 after failure. Critical pressure = 69MPa.....	39

Figure 38 - Fiber stresses, development with increasing pressure, D=11mm, Location 1. Compressive fiber failure predicted at about 180MPa pressure, occurring before instability.....	46
Figure 39 - Fiber stresses, development with increasing pressure, D=11mm, Location 2. Compressive fiber failure predicted at about 190MPa pressure, occurring before instability.....	46
Figure 40 - Transverse stresses, development with increasing pressure, D=11mm, Location 1. Instability predicted at about 420MPa pressure, before Puck criterion predicts failure. ....	47
Figure 41 - Transverse stresses, development with increasing pressure, D=11mm, Location 2. Instability predicted at about 530MPa pressure, before Puck criterion predicts failure. ....	47
Figure 42 – Rendered image of hoop fiber layer in specimen nr8, with 200x enhancement. Estimated volume fraction: 0,554.....	48
Figure 43 – Rendered image of hoop fiber layer in specimen nr8, with 500x enhancement. The volume fraction calculated is considered to be somewhat conservative due to the dark edges. Second part of the used section. Estimated volume fraction: 0,543. ....	49
Figure 44 – Rendered image of hoop fiber layer in specimen nr8, with 500x enhancement. The volume fraction calculated is considered to be somewhat high as space between fibers from parts of picture is quite bright. Second part of the used section. Estimated volume fraction: 0,623. ....	49
Figure 45 – Rendered image of hoop fiber layer in specimen nr8, with 500x enhancement. The volume fraction calculated is considered to be somewhat conservative due to the dark edges. Second part of the used section. Estimated volume fraction: 0,508. ....	50
Figure 46 – Rendered image of hoop fiber layer in specimen nr8, with 500x enhancement. The volume fraction calculated is considered to be somewhat high as space between fibers from parts of picture is quite bright. Second part of the used section. Estimated volume fraction: 0,596. ....	50
Figure 47 – Rendered image of hoop fiber layer in specimen nr2, with 50x enhancement. Estimated volume fraction: 0,534.....	51
Figure 48 – Rendered image of hoop fiber layer in specimen nr2, with 100x enhancement. Estimated volume fraction: 0,558.....	52
Figure 49 – Rendered image of hoop fiber layer in specimen nr2, with 500x enhancement. Estimated volume fraction: 0,530.....	52

## Tables

Table 1 - Load, temperature and physical requirements .....	2
Table 2 – Properties of a transversely isotropic UD carbon composite material.....	4
Table 3 – Failure strength parameters .....	6
Table 4 - Critical bending radius results for the two different submerged weights. The bending radius has been calculated with background in the failure criterions set in section 1.5 .....	9
Table 5 – Maximum stresses and strains for the required bending radius of 4200mm, given in longitudinal direction, of various dimensions. (0° represent the longitudinal layer and 90° the hoop layer).....	10
Table 6 – Longitudinal and bending stiffness for tubes with equal thickness of hoop and longitudinal fibers. ....	11
Table 7 - Load factor for tubes composed of only hoop fibers and only longitudinal fibers. ....	20
Table 8 - Results of Linear perturbation analyses, both layup models .....	20
Table 9 - Load factor results for possible specimen dimensions.....	21
Table 10 – Comparing axisymmetric vs. RIKS, D=16mm, P=100MPa, equal thickness of hoop- and longitudinal fibers. Benchmark fields are comparable with values in last row (element nr 30 in axisymmetric model). Lowest element nr is innermost in the structure, and highest element nr is at the outermost location in the structure. ....	23
Table 11 - Comparison, axisymmetric vs. RIKS, D=22mm, P=100MPa, equal thickness of hoop- and longitudinal fibers. ....	26
Table 12 - Weights of scaled tube with original dimensions D=22mm and d=12mm.....	29
Table 13 - Data on components used to make specimens .....	30
Table 14 – Critical pressure for all specimens .....	37
Table 15 - Longitudinal and bending stiffness for 0 g/m tubes with layup model 2. ....	44
Table 16 - Longitudinal and bending stiffness for 50 g/m tubes with layup model 2. ....	44
Table 17 - Specimen data .....	45

# 1 Introduction

Advanced composite materials and structures which have low weight, high stiffness, high strength and chemical resistance can be utilized in order to obtain low weight high capacity tubes for well intervention. Such tubes, when deployed in oil and gas wells with high temperature, high pressure and aggressive environment, must be designed with respect to external pressure capacity, longitudinal stiffness and strength capacity, buckling capacity, thermal dependency, and specific thermal and chemical resistance.

The high specific strength and corrosion resistance of composite materials have led to an increasing industrial use. Composite tubes started in the early 1990s to be considered for the marine and oil industry as an alternative for transportation of fluids, and research for this purpose was done such as the work of J.Mistry et.al. [1]. The most critical factor for such tubes has shown to be buckling. Work on the compressive-compressive stress state of composite cylinders was conducted [2]. More recent work on composite cylinders under external pressure has been more on optimizing the structure of the cylinders, such as the work of Hernández-Moreno et.al. on the influence of winding pattern on mechanical behavior [3].

During the background search for this thesis it was found that very little work had been carried out on thick walled composite cylinders. In all of the aforementioned articles the authors have conducted experiments on thin walled cylinders modeled mainly as shells. Some work on cylinders of intermediate thickness has been conducted, such as the work of C.-J. Moon et.al. [4], where experiments on intermediate thick tubes have been conducted for use in subsea vehicles.

The shared feature of all the work carried out in the aforementioned papers is that they all evolve around tubular structures. The work of J.Mistry[5] showed that the diameter to thickness ratios is inversely proportional to the critical pressure. Furthermore, in the same paper, it is shown that the length to diameter ratio also influence the critical pressure, especially for small ratios. Because of the large diameter to thickness ratios the structures collapse for low to moderate pressures.

In this thesis it has been conducted both an analytical and experimental study of the behavior of thick walled filament wound composite tubes, with both relatively high length to diameter ratio and a low diameter to thickness ratio, subjected to high external pressure.

## 1.1 Requirement specification

Necessary requirements for the tube are given in Table 1.

<b>Loads and temperature requirements</b>	
Temperature (max)	150 °C
Tensile load capacity	> 50 kN
Pressure capacity (external)	1000 bar = 100 MPa
Bending Radius	4200 mm
<b>Physical properties &amp; dimensions</b>	
Outer Diameter max	22 mm, preferred <20 mm
Submerged weight pr length in water	<50 g/m

**Table 1 - Load, temperature and physical requirements**

The tube shall have as high as possible bending stiffness. The failure bending radius should be as small as possible, as a safety factor compared to the requirement of 4200mm is necessary. The tube shall survive 1000 bar at 150C for more than 48 hours, and a general chemical resistance is demanded (material chemistry).

A solid rod with 15 mm diameter and a CFRP material has a submerged weight per length equal to 106 g/m. In order to reduce the frictional force in horizontal well the submerged weight must be reduced. Additional weight of fiber optics which contributes by approximately 15 g/m must be included.

The temperature requirement is considered beyond the scope of this thesis and is not subject to any calculations or testing. This is a requirement which needs further attention in a later stage of the development process.

Fatigue has not been considered (i.e. the requirement of 48h survival) due to lack of data in wells on the subject and is considered to be beyond the scope of this thesis.

### 1.1.1 Load cases

The tube will principally undertake 3 load cases:

1. Crushing: While fed into the well, the tube will be squeezed between two feeding bands. This could cause crushing.
2. Collapse/Buckling: While fed into the well (and during operation) the tube inside the well will undertake an outside overpressure and a longitudinal compressive force due to this pressure. The necessary pressure the tube need to withstand is given to be  $P=100\text{MPa}$ .
3. Upon retrieval the tube undertakes the same outside overpressure of 100MPa together with a longitudinal tensile force of  $F=50\text{kN}$ . The tube can in the same way be, together with the pressure, subjected to a compressive force of  $F=50\text{kN}$  while fed into the wall.

Notice that the forces mentioned in the load cases above are absolute, meaning they represent the total longitudinal forces the tube will be subjected to.

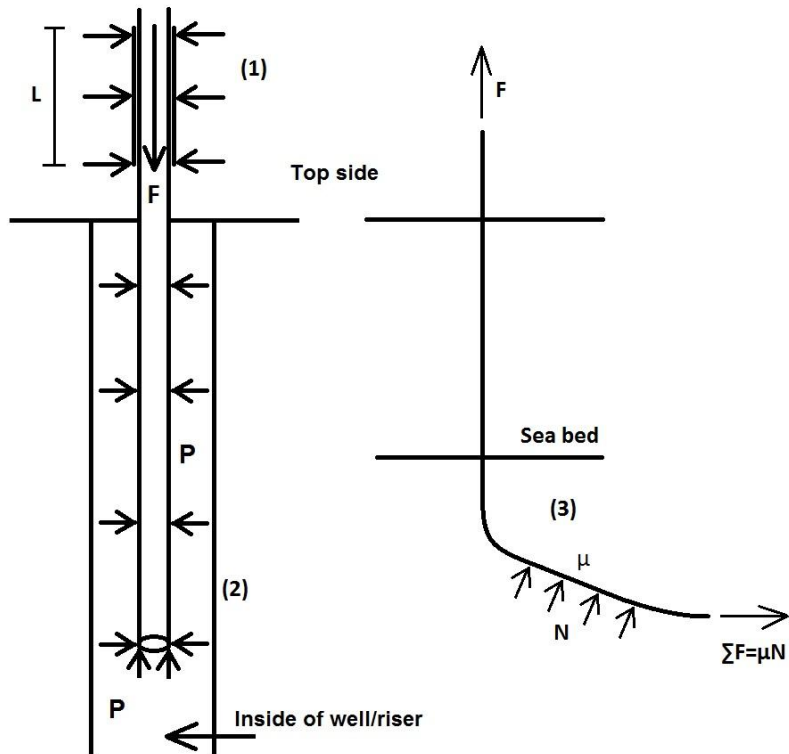


**Figure 1 - The different load cases the tube undertakes. The numbers represent the different load cases described above.**

Crushing is a load case which there is a number of unknown parameters. This load case was therefore considered beyond the scope of this thesis.

## 1.2 Material properties

For all calculations and analysis it was used typical material property values for a transversely isotropic uni-directional carbon composite material. The material properties are given in Table 2.



CFRP material properties	
E1 [MPa]	140000
E2 = E3 [MPa]	8000
v12 = v13	0,3
v23	0,55
G12 = G13 [MPa]	4000
G23 [MPa]	2581
$\rho$ [kg/m <sup>3</sup> ]	1600

**Table 2 – Properties of a transversely isotropic UD carbon composite material.**

It would have been convenient for benchmarking purposes to use material properties of the rod in use today, or the properties of the specimen. However, neither of these was known at the early stages of analysis. Set properties were used throughout all analysis.

### 1.3 Weight

Equation (1.1) describes the relation between the outer (D) and inner (d) diameter for a given submerged weight in water. The weight of the fiber optics was set in accordance with the requirement specification to be constant and equal to 15 g/m. The relation for two specific weights is shown in Figure 2.

$$\frac{D^2 - d^2}{4} \pi \cdot \rho_{CFRP} - \frac{D^2}{4} \pi \cdot \rho_{water} + 15 \frac{g}{m} = SubmergedWeight \quad (1.1)$$

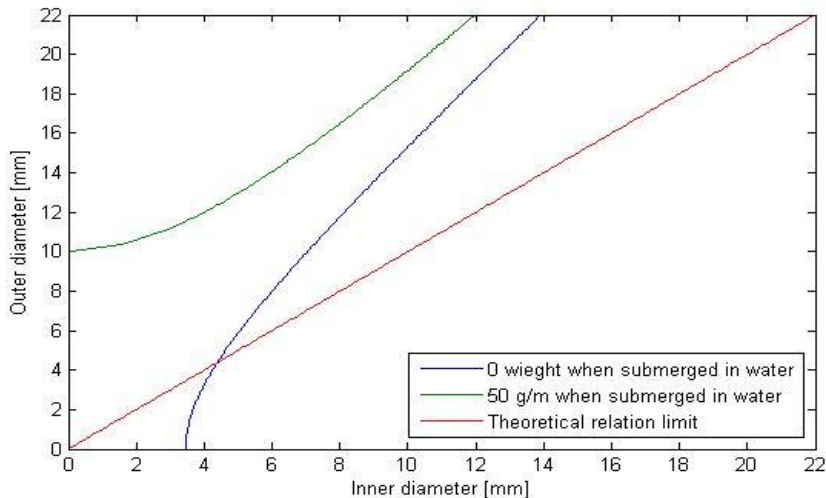


**Figure 2 – Relation between inner and outer diameter of the tube to achieve a satisfactory submerged weight. The red line represents an infinite thin tube.**

## 1.4 Layups

A number of layups and winding angles were considered, such as  $\pm 55^\circ$  wound structures. This structure would give good results considering strength in radial direction, and excellent torsion properties. However, it also would give relatively low longitudinal and bending stiffness, which is not fulfilling the specified requirement, and was therefore not used.

Multilayered layups were considered as this would give better resistance against crack development than UD or few layers. The challenge with a multilayered tube would be the production process which would need to have as many production stages as there would be layers.

It was chosen a layup with an innermost hoop layer with a longitudinal layer on the outside. This layup will maintain the requirement of obtaining a high longitudinal stiffness and to obtain high strength in the radial direction. The hoop layer will be responsible of handling the pressure and it does not matter much if it is outermost or innermost in the structure. To obtain highest possible bending stiffness the longitudinal layer must be on the outside. Another reason is the manufacturing perspective. Today's rod is made by pultrusion which gives a smooth surface, which is desired to keep friction between tube and well low.

Two different layups was considered. Both layups consists of an inner layer with hoop-fibers and an outer layer of longitudinal fibers. The two models are shown in Figure 3. The reason for the essentially similar layups, and only differ the ratio between hoop and longitudinal thickness, was to see how differing this ratio would affect the stress distribution.

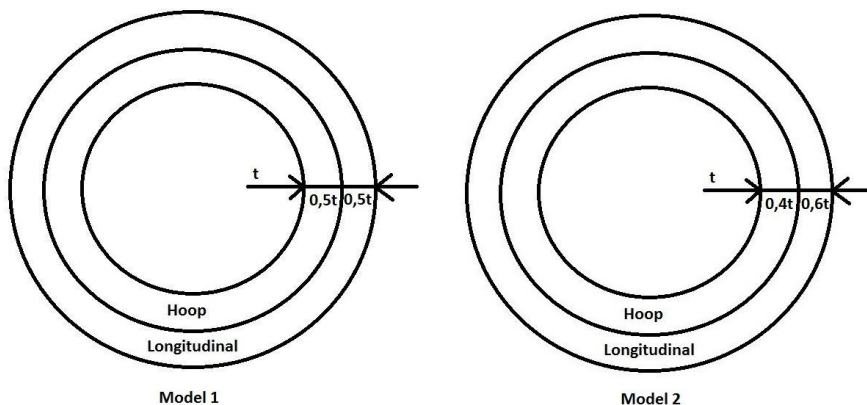


Figure 3 – The two different layup models.

The geometric dimensions considered are between 14mm and 22mm in outer diameter. The diameter of 22mm is given by the requirement specification, and the lower limit of 14mm diameter is only given by the fact that today's rod is 15mm in diameter and thus it seemed natural to have something about the same size and even smaller to establish a sort of worst case scenario.

In the analyses the material was normalized and oriented to the respective fiber directions. The hoop layer was set to  $\pm 88^\circ$  winding angle as an angle of  $90^\circ$  was not expected to be practically feasible. The longitudinal layer was set to an angle of  $0^\circ$ .

### 1.5 Failure Criteria

It was assumed that there are no coupling between the stress parallel to the fiber and the stresses perpendicular to the fiber (as there theoretically are no shear stresses) due to the axisymmetric geometry and material properties and to the assumption that the tube is infinitely long.

Failure parameters were defined; values are achievable for an industrial composite.

Failure criteria	Strength [MPa]
$R_{\parallel}^t$	1000
$R_{\parallel}^c$	800
$R_{\perp}^t$	50
$R_{\perp}^c$	150

**Table 3 – Failure strength parameters**

For fiber fracture (FF) the maximum stress criterion, relation of equations(1.2), was chosen as the failure criterion. A more sophisticated criterion for FF which takes into account secondary effects of 3-dimensional stressing could have been used. However, this approach is found sufficient for preliminary analysis. [6]

$$\begin{aligned} \frac{\sigma_1}{R_{\parallel}^t} &= 1 & \text{if } \sigma_1 > 0 \\ \frac{-\sigma_1}{R_{\parallel}^c} &= 1 & \text{if } \sigma_1 < 0 \end{aligned} \tag{1.2}$$

For the inter fiber fracture (IFF) criterion there are many failure criteria which could be applied. However, as the stress state is in the third quadrant (compressive-compressive) of the stress chart there are many criteria which simply do not correspond with reality. An example the Tsai-Wu criterion would for this application be

much too conservative. Since in this case it is also a 3-dimensional state of stress, all 2-D criteria are not applicable.

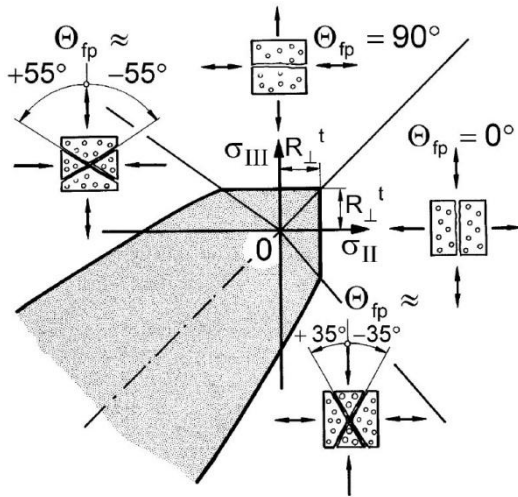


**Figure 4 - Pucks IFF criterion (Analysis of Failure in Fiber Polymer Laminates, 2008 [6])**

The chosen criterion to assess IFF was the Puck criterion [6], illustrated in Figure 4. This criterion is perhaps one of the most acknowledged ones, at least for the third stress quadrant. Other criteria such as the Hashin criterion could have been applied, but as the scope of this thesis is to conduct a feasibility study, it is considered redundant to use more than one failure criterion for the same stress parameters.

### 1.6 Bending radius

A critical bending radius of maximum 4200mm has to be obtained (see section 1.1 about the requirements specification). As stress will mainly be in the axial direction, the hoop layer will undertake mainly transversal stress and the longitudinal layer will undertake stress in fiber direction.

To simplify we assume a linear distribution of strains and stresses as shown in Figure 5. Furthermore it is assumed that  $\epsilon_y$  is negligible compared to  $\epsilon_x$ . A justification for this is that these calculations are to investigate if the bending radius is going to be a problem for the structure, not to give an accurate prediction of the final critical bending radius.

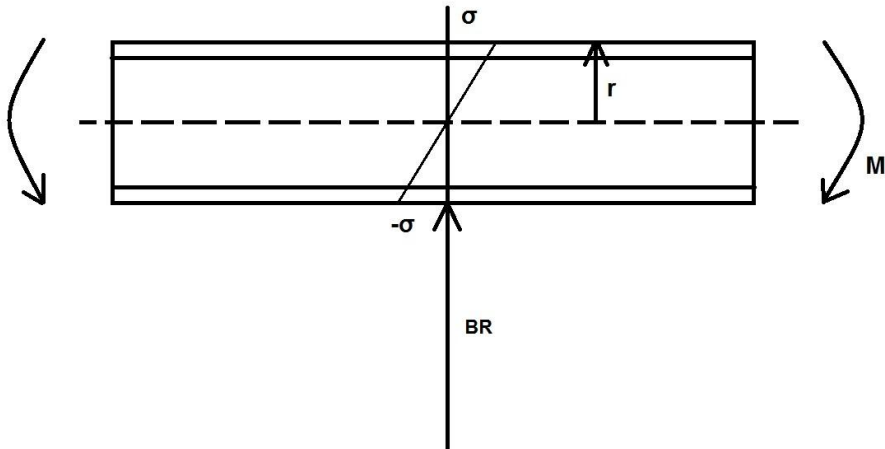


**Figure 5 – Model for minimum bending radius**

The stress can be found by simplifying and using Hooke's law.

$$\sigma_x = E_x \varepsilon_x \quad (1.3)$$

where \$x\$ represent global orientation in the axial direction, and

$$\varepsilon_x = r\kappa = \frac{r}{BR} \quad (1.4)$$

By combining equations (1.3) & (1.4) we get the bending radius \$BR\$;

$$BR = \frac{E_x}{\sigma_x} r \quad (1.5)$$

By substituting \$\sigma\_x\$ in (1.5) with each of the governing failure strengths in Table 3, and using the material properties given in Table 2, we get the critical bending radius \$BR\_c\$ given in Table 4.

Both the minimum bending radius for the given maximum stresses and the stress given by the bending radius required is presented here. The requirement of 4200m as a minimum bending radius implies that in reality a smaller minimum bending radius must be obtained such that a safety factor can be established.

0 g/m Submerged Weight				50 g/m Submerged Weight			
D [mm]	d [mm]	$BR_c(R'_\perp)$ [mm]	$BR_c(R''_\parallel)$ [mm]	D [mm]	d [mm]	$BR_c(R'_\perp)$ [mm]	$BR_c(R''_\parallel)$ [mm]
14	9,24	930	1225	14	6,8	832	1225
15	9,8	992	1313	15	7,5	900	1313
16	10,37	1055	1400	16	8,3	972	1400
17	10,96	1118	1488	17	9	1040	1488
18	11,55	1182	1575	18	9,7	1108	1575
19	12,13	1245	1663	19	10,4	1176	1663
20	12,7	1308	1750	20	11	1240	1750
21	13,3	1372	1838	21	11,7	1308	1838
22	13,9	1436	1925	22	12,4	1376	1925

**Table 4 - Critical bending radius results for the two different submerged weights. The bending radius has been calculated with background in the failure criterions set in section 1.5**

From Table 3 it is obvious that the governing failure modes would be either  $R''_\parallel$  or  $R'_\perp$ . For the layer with longitudinal fibers the governing failure mode is  $R''_\parallel$ , and for hoop fibers it is  $R'_\perp$ .

For the longitudinal fiber layer the results in both weights are equal since the outer diameter is the same. For the hoop layer the results differs bit between the two weights as the outer diameter in the hoop layer is different. Nevertheless it is evident that it is compression of the longitudinal fibers which become the governing parameter for the bending radius.

Also seen from Table 4 is that for all considered dimensions of the tube, the critical bending radius is kept well below the demand on 4200mm.

Assuming that the tube will be stored on a drum with a radius of 4200mm the maximum stresses and strains resulting from this will be as described in Table 5.

BR = 4200mm, 0 g/m Submerged Weight					
D [mm]	d [mm]	ε 0°ply	σ 0° ply	ε 90°ply	σ 90° ply
14	9,24	1,67E-03	234,5	1,38E-03	11,1
15	9,8	1,79E-03	251,3	1,48E-03	11,9
16	10,37	1,90E-03	268,0	1,57E-03	12,6
17	10,96	2,02E-03	284,8	1,66E-03	13,4
18	11,55	2,14E-03	301,5	1,76E-03	14,1
19	12,13	2,26E-03	318,3	1,85E-03	14,9
20	12,7	2,38E-03	335,1	1,95E-03	15,7
21	13,3	2,50E-03	351,8	2,04E-03	16,4
22	13,9	2,62E-03	368,6	2,14E-03	17,2

**Table 5 – Maximum stresses and strains for the required bending radius of 4200mm, given in longitudinal direction, of various dimensions. (0° represent the longitudinal layer and 90° the hoop layer)**

The stresses and strains for a tube with a submerged weight of 50 g/m gave the same results for the longitudinal ply and slightly lower values for the hoop ply, compared to the tube of 0 g/m weight. The stress is far below the failure criteria set in subsection 1.5. The strains are only presented here to illustrate the strain magnitude. Strains are not used for failure analysis.

### 1.7 Longitudinal- and bending- stiffness

The requirement for the bending stiffness is not specified to be anything else than *as high as possible*, and the longitudinal stiffness has not been subject in the requirements.

The longitudinal stiffness  $K$  of the tube follows the equation;

$$K = AE \quad (1.6)$$

where  $A$  is the total cross sectional area of the tube. The longitudinal elastic moduli  $E$  are found by;

$$E = \frac{1}{A} \sum_{i=1}^n E_i \cdot A_i \quad (1.7)$$

where  $n$  is the number of plies,  $A_i$  is the cross-sectional area and  $E_i$  is the stiffness in (global) longitudinal direction for each ply.

The bending stiffness  $k$  is given by;

$$k = \sum_{i=1}^n E_i I_i \quad (1.8)$$

where  $n$  is the number of plies,  $E_i$  is the longitudinal stiffness as before and  $I_i$  is the 2<sup>nd</sup> areal moment for each ply, given by;

$$I_i = \frac{\pi}{4} (D_i^4 - d_i^4) \quad (1.9)$$

where  $D$  is the outer diameter and  $d$  is the inner diameter of the tube.

D [mm]	Submerged weight with fiber optics [g/m]	Longitudinal stiffness, K=A*E [MPa]	Bending stiffness [MPa*mm <sup>4</sup> ]
14	0,07	7,02E+06	1,43E+08
15	0,34	8,20E+06	1,91E+08
16	0,50	9,45E+06	2,50E+08
17	0,24	1,08E+07	3,21E+08
18	0,04	1,22E+07	4,06E+08
19	0,22	1,37E+07	5,07E+08
20	0,81	1,53E+07	6,26E+08
21	0,53	1,69E+07	7,64E+08
22	0,28	1,86E+07	9,23E+08
<b>Benchmark: Today's Carbon Rod</b>			
15	116,00	2,43E+07	3,14E+08
D [mm]	Submerged weight with fiber optics [g/m]	Longitudinal stiffness, K=A*E [MPa]	Bending stiffness [MPa*mm <sup>4</sup> ]
14	49,26	1,00E+07	1,87E+08
15	50,34	1,13E+07	2,43E+08
16	49,07	1,24E+07	3,07E+08
17	49,40	1,37E+07	3,86E+08
18	49,44	1,51E+07	4,80E+08
19	49,20	1,66E+07	5,88E+08
20	51,44	1,83E+07	7,20E+08
21	50,80	1,99E+07	8,66E+08
22	49,86	2,16E+07	1,03E+09

**Table 6 – Longitudinal and bending stiffness for tubes with equal thickness of hoop and longitudinal fibers.**

The additional thickness ratio was considered. The same calculations regarding longitudinal and bending stiffness was done, and the results were respectively 15-16% and 11-13% higher. These results are found in Appendix 1.



Comparison of the longitudinal stiffness with today's rod we see that, unless using quite large outer diameters, a moderate to considerable longitudinal stiffness decrease. This is due to the new design is hollow and that half the thickness now has a much lower longitudinal stiffness.

However, even though the longitudinal stiffness has declined, the bending stiffness of the tubes larger than 16mm in diameter will all surpass today's rod.

## **2 Numerical modeling**

For all the numerical modeling and analysis the FEM software *Abaqus 6.10* [7] was used.

The objective of the numerical analysis was to obtain stress results to conclude if it is feasible to make a tube withstand the high pressures, to detect points of instability and to identify buckling modes and critical pressures.

### **2.1 Axisymmetric model**

The first step in analysis was to find out how the relation between stresses changes with changing geometric relations for the required pressure of 100MPa, and if the stresses were at least reasonable within the set criterions. The varying parameters in geometry were the outer diameter, the ratio between outer and inner diameter and the two different layups shown in Figure 3. As there were several parameters, many analyses were required. An axisymmetric model was chosen due to its numerical efficiency.

#### **2.1.1 Mesh**

The element used for all analysis with the axisymmetric model is the *CAX4R* [7], which means it is a 4-node bilinear axisymmetric quadrilateral element with reduced integration and hourglass control. It was used elements that were evenly distributed through the thickness and had a size within the range of 0,1 to 0,3 (dependent on wall thickness of tube). Only one element used in the longitudinal direction. Aspect ratio of elements was kept below 3.



**Figure 6 - Meshed axisymmetric model**

### 2.1.2 Loads and boundary conditions

A reference point was created and the axial load was set in this point. The reference point was coupled with the end of the cylinder with a constraint equation. Pressure was set on the outside of the model.

It is given that the structure must be able to undertake an outside overpressure of 100MPa. This is pressure was used in all load cases in addition to a longitudinal force. In *load case 3* it is given an axial force of 50kN, which can either be compressive or tensile.

The only boundary condition was to arrest the side opposite of the force loaded side in axial direction as the axisymmetric model itself sets the rest of the necessary boundary conditions.

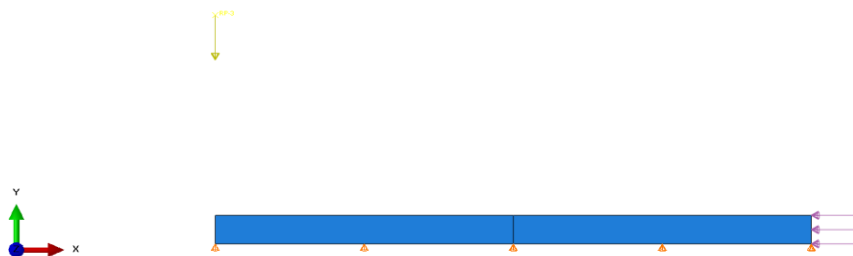


**Figure 7 - Loads and boundary conditions on axisymmetric model**

## 2.2 3D models

When setting up both buckling models an assumption was made that the ruling buckling mode would be collapse due to implosion. Further the collapse would initiate as an ellipse. This assumption conflicts from earlier results found by e.g. Moon[4] as the governing collapse in his work was wave three (mode 3), a collapse shaped like a triangle. However, the assumption is considered valid as the tube considered in this case will also be subjected to bending during operation (will be pushed around bends inside the wells). This bending will give the initial geometric imperfection, later discussed in section 2.2.2, which dictates a collapse as assumed. All of the referenced

work worked under the boundary conditions that their constructions was not subjected to any bending loads or displacements, and would therefore not collapse in the same matter.

Two different models were used to analyze buckling effects. The linear perturbation was chosen because of its efficiency and to get an overview of how much loading the different specifications can handle. The second buckling model was done by RIKS analysis and was chosen to get results of the stress behavior as the pressure increases.

### 2.2.1 Linear perturbation model & mesh

Layups used in this analysis were the same as for the axisymmetric model, see Figure 3. To simplify the model it was chosen to only look at a half section of the tube.

To mesh the model only one element was used in the longitudinal direction. Through the thickness it was used elements of size between 0,25 and 0,5. The type of element used was *C3D20*; a 20-node quadratic brick [7]. The elements were applied by swept meshing with advancing front. Aspect ratio of elements was kept below 2.

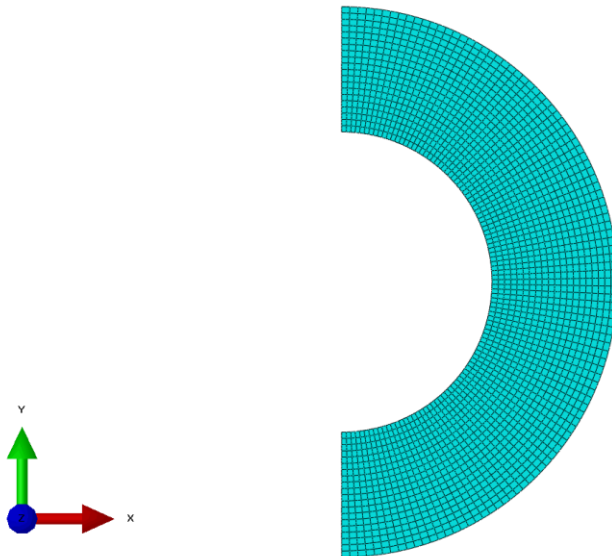
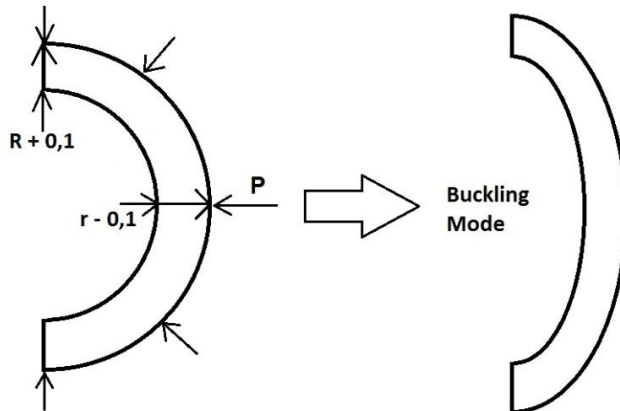


Figure 8 - Buckle models mesh

### 2.2.2 RIKS model & mesh

To get initiation of buckling in the RIKS analysis an imperfection of the geometry must be introduced. The imperfection was to introduce a slightly elliptic shape as shown in Figure 9. This was done by increasing and decreasing the elliptic radiuses in respect to the original radius.



**Figure 9 - Introduction of geometric imperfection in RIKS model.**

The model was meshed in the same way as for the Linear Perturbation model (see subsection 2.2.1 and Figure 8). The type of element used was *C3D8R*; an 8-node linear brick with reduced integration and hourglass control [7], applied by structured meshing. Aspect ratio of elements was kept below 2.

### 2.2.3 Loads and boundary conditions in buckling models

The loads used in both buckling models were a unit load (1MPa) of the outside pressure and a compressive longitudinal force given as a product of that pressure and geometry of the tube. The reason was to get results of the linear perturbation analysis, the *Load Factor*, to be equal to the buckling load. For the RIKS analysis there was no particular reason for using a unit load except for convenience (already calculated longitudinal forces from linear perturbation).

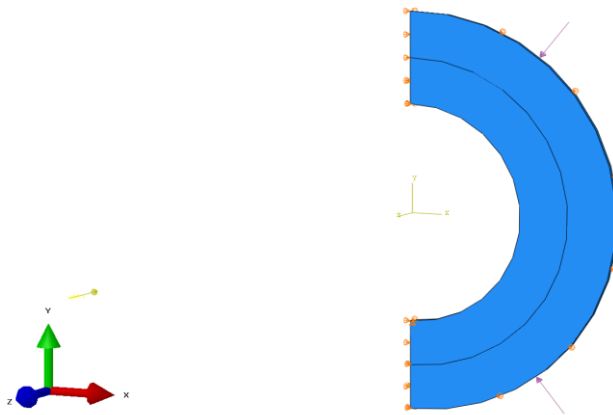


**Figure 10 - Loads and boundary conditions on buckling models**

To get an evenly distributed compressive force a reference point was made and linked to the end surface with a *constraint equation*. The compressive force was established as a *concentrated force* in the reference point.

Three boundary conditions were established. One locking the end surface opposite to the side linked to the reference point (Z-direction). One locking the surfaces made from sectioning the tube (X-direction). To prevent rigid body motion in the analysis a point on the inside of the tube, at the corner where the two other boundary conditions intersect, was locked in Y-direction. All directions are given in global coordinates (see Figure 10).

### 3 Numerical results

During this section the results of the abaqus simulations will be presented.

#### 3.1 Axisymmetric Model

Throughout these analyses a few clear relations between the physical features of the tube and the transversal stresses emerged. In this context the transversal stresses is the relation between  $\sigma_2$  and  $\sigma_3$ . These relations only apply to the hoop layer as the transversal stresses in the longitudinal fibers seemed to be fairly constant with both various axial loading and varying physical features (The collection of data points at the lower left end of the curves in Figure 12 and Figure 13).

In Figure 11 the maximum fiber stress predicted when the tube is under 50kN compressive loading (in addition to the outside pressure) is presented as a function of the outer diameter for two specific submerged weights. This represents the most

exposed load case (described in section 1.1.1), as this give the highest absolute value in compressive stress.

At the start of this work there was a misunderstanding when considering the weight requirement and therefore the results in Figure 11 are presented for tubes of 65 g/m instead of 50 g/m. However, the results for any submerged weight can be approximated by interpolating the results given in the figure.

Notice that the maximum fiber stress curves for the two orientations have an intersection point where the stresses are equal, and that this point is for the same outer diameter of 19mm for both considered weights. This could be interpreted as that there exist an optimum dimension for utilizing the composites strength in the whole structure of the tube.

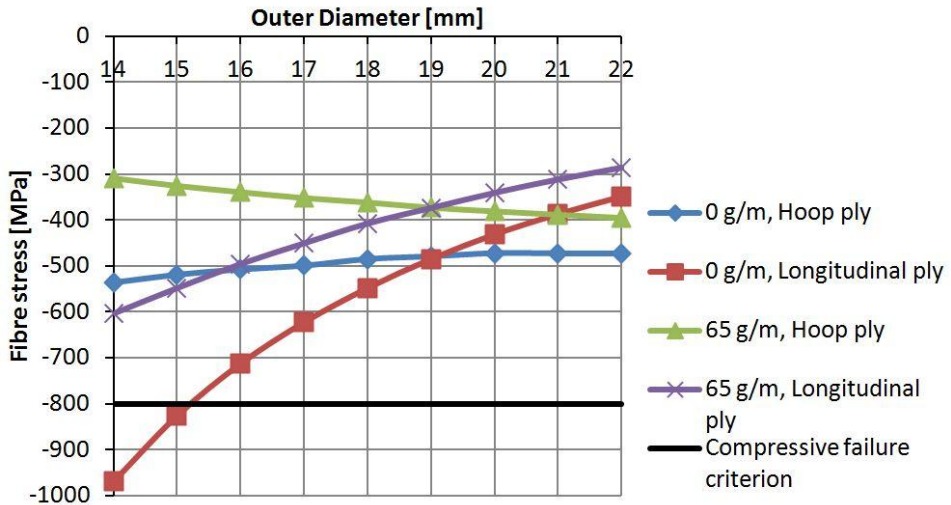
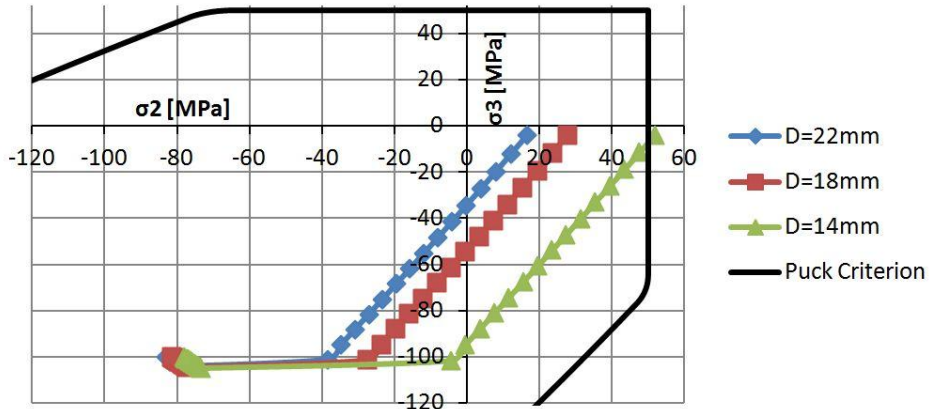


**Figure 11 - Maximum fiber stresses predicted for each layer as a function of outer diameter, subjected to a compressive force of 50kN (in addition to the outside pressure).**

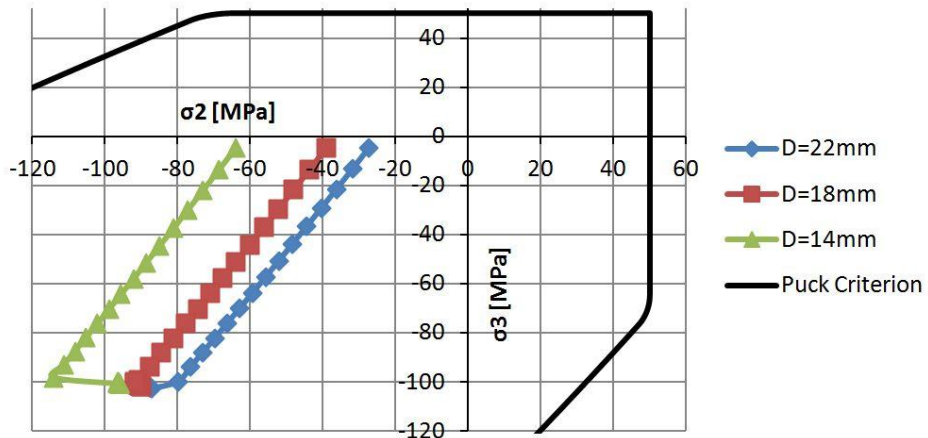
Another conclusion to draw from the above figure is that tubes with both low weight and low diameter can expect failure in the longitudinal ply.

Figure 12 and Figure 13 shows the two most exposed stress conditions found during the analyses. All other analyses showed a relation between  $\sigma_2$  and  $\sigma_3$  where these stresses are closer to equal. The points on the curves represent data points from elements through the thickness of the tube. The point closest to the horizontal axis is closest to the center of the tube (meaning that the gradient line represents stress through the hoop winded layer). The collection of points at the bottom of each of the gradient lines

represents the outer longitudinal layer. It can be seen that the gradient of each of the lines seems fairly unchanged.



**Figure 12 - Transversal stresses through thickness in tubes with a submerged weight of 0 g/m and equal thickness of hoop and longitudinal fibers, undertaking 50kN tensile force.**



**Figure 13 - Transversal stresses through thickness in tubes with a submerged weight of 0 g/m and equal thickness of hoop and longitudinal fibers, undertaking 50kN in compressive force**

The figures showing the relation between the transversal stresses show that the only point outside the set failure criterion is the innermost point in the 14mm tube when subjected to 50kN tensile force. This tube represents the dimensional extreme as any smaller diameters are after this analysis considered unfeasible, and an even lighter tube would lead to undesired buoyancy.

### 3.1.1 Relations between physical features and stress

Given an outside pressure of 100MPa it was no surprise to see that the longitudinal fibers layer had a more or less constant compressive stress through the thickness ( $\sigma_3$ ). Also the stress through the thickness of the hoop layer stayed unchanged. This was not mentionable inflicted by changing neither the longitudinal loading nor the geometric dimensions of the tube.

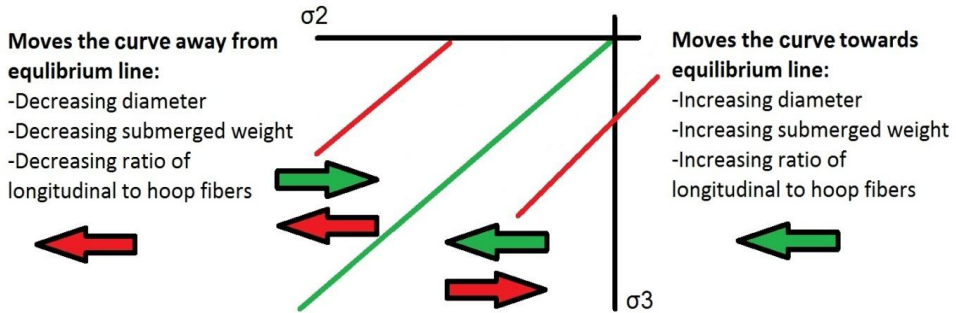


**Figure 14 - General behavior of the transversal stresses through the thickness. The green lines represent possible states of stress found in the analyses.**

There seemed to be 3 parameters regarding physical features which had significant impact on  $\sigma_2$  for the hoop winded fiber layer. These factors are: 1. Outer diameter of the tube (a change in outer diameter and a corresponding change in inner diameter so that the submerged weight stay constant), 2. submerged weight (outer to inner diameter ratio) and 3. longitudinal to hoop fiber ratio. An increase in any of these three parameters will move the stress curve towards equilibrium between  $\sigma_2$  and  $\sigma_3$ , and a decrease will move the curve away from equilibrium. Figure 14 illustrates how the stress curve move with changes in physical features depending on which side of the equilibrium the stress curve is situated. In this context the indexes 2 and 3 represent local material orientation.

### 3.2 Linear perturbation buckling model

The first analysis with this model was made to find the effect of using longitudinal fibers versus hoop fibers exclusively. A benchmark for the existing rod with this model would not give reasonable results as a solid rod would not be subject to the same buckling behavior. The results in Table 7 clearly show that hoop fibers endure the loading condition better than longitudinal fibers. All tests showed collapse due to the expected buckling mode explained in section 2.2.



	D [mm]	d [mm]	Sub, weight with fiber optics [g/m]	Load Factor
Only longitudinal	14	6,8	49,26	500
Only hoop	14	6,8	49,26	1760

**Table 7 - Load factor for tubes composed of only hoop fibers and only longitudinal fibers.**

Equal thickness of longitudinal and hoop fibers				60% of thickness with longitudinal fibers, 40% of thickness with hoop fibers			
D [mm]	d [mm]	Sub. weight with fiber optics [g/m]	Load factor	D [mm]	d [mm]	Sub. weight with fiber optics [g/m]	Load factor
14	6,8	49,26	1130	14	6,8	49,26	1001
18	9,7	49,44	842	18	9,7	49,44	741
22	12,4	49,86	726	22	12,4	49,86	635
14	9,24	0,07	359	14	9,24	0,07	307
18	11,55	0,04	418	18	11,55	0,04	360
22	13,9	0,28	452	22	13,9	0,28	390

**Table 8 - Results of Linear perturbation analyses, both layup models**

Considering the results in Table 8 the load factor for tubes with the highest hoop to longitudinal thickness ratio exhibits the highest load factors. The tubes of submerged weight 50 g/m show a significant drop in the load factor with rising outer diameter, and a slightly increasing load factor is observed for 0 g/m tubes with increasing diameter. The ratio between outer and inner diameter change differently with increasing diameter for the two submerged weights considered here, which is the reason for the differing behavior.

Notice that the load factor indicates at what pressure (in MPa) the structure will collapse. These results therefore show that a collapse at the given pressure of 100MPa will not happen for any of the tubes. In the worst cases a safety-factor of about 3 is obtained.

The predicted failure is due to collapse (implosion) and is therefore governed by the hoop layer. Further work has subsequently only considered the model with the highest relative thickness of hoop fibers, which is equal thickness of hoop and longitudinal fibers.

### 3.2.1 Choosing specimen dimensions

The reason for choosing an inner diameter of 12mm is described in section 4, along with information on specimen dimensions, production and other details.

D [mm]	d [mm]	Sub. weight with fibreoptics [g/m]	Load factor	Largest element aspect ratio
16	12	-45,32	147	1,16
17	12	-29,77	239	1,19
18	12	-13,27	344	1,23
19	12	4,16	458	1,26
20	12	22,54	576	1,3
21	12	41,86	697	1,34
22	12	62,12	819	1,39

**Table 9 - Load factor results for possible specimen dimensions**

From the results in Table 9 all the load factors are above 100. This means that from the results given from this analysis, a pressure of close to 1500 bar is needed to get even the thinnest of the considered specimen dimensions to collapse.

### 3.3 RIKS Buckling Model

To log the pressure in the RIKS model it was chosen to use the S33 (stress through thickness) values of the centroid, as it was used 8 node elements, of an element at the outermost side of the structure. This is not completely accurate values as the stress is then logged from the center of the element. Since the elements were so small the error (the difference between the measured pressure and the real pressure) was assumed to be negligible. To back up this assumption, a check of the error was made by finding the total reaction force at the flat surface of symmetry, and then calculating the pressure based on this force, following equation(3.1). The error in S33 compared to the calculated pressure were about 1,5%, hence insignificant. The method of calculating the pressure is showed in Figure 15.

$$\sum F = P \cdot D \cdot t \quad (3.1)$$

Upon extraction of results two different locations of the structure were used, as these two locations give the stress extremes of the structure, shown to the right in Figure 15. Stress values from six elements through the thickness were extracted.

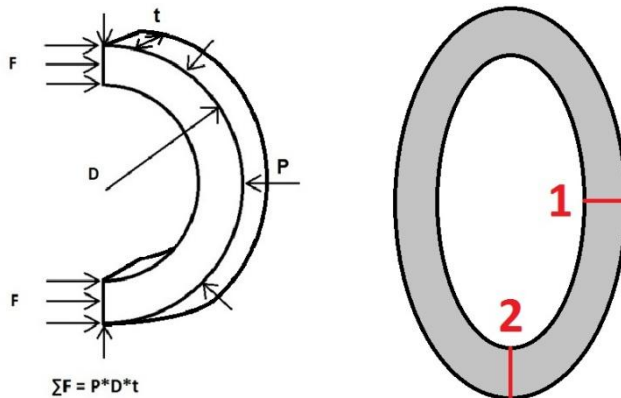


**Figure 15 - Pressure validation shown to the left and the two locations for extraction of stress data shown to the right.**

A benchmark for the imperfection in geometry was executed with a geometric imperfection of just 10% of the original imperfection (switching from  $\pm 0,1\text{mm}$  to  $\pm 0,01\text{mm}$  in Figure 9). It was found that the development of the transverse stress in comparison with increasing pressure changed significantly. The benchmark showed a more linear development to the point of instability/collapse, which not only happens at a noticeable higher pressure but also give a more sudden instability (Figure 19).

### 3.3.1 Analysis of tube with specimen dimensions

Considering characteristics in the development of stress in fiber direction with increasing pressure (Figure 16 and Figure 17), for the selected elements, the stress through the thickness in the two locations show no major differences. The largest difference is found in the development of stress in the middle of the hoop ply (referred to as *90 ply Mid* in all stress curve figures), where it is seen that the stress overstep the compressive stress limit in location 2 (Figure 17). However, when considering fiber failure due to compressive stress, the analysis show that it is the outermost hoop layer (referred to as *90 ply Outer* in Figure 16) at location 1 and the innermost hoop layer (referred to as *90 ply Inner* in Figure 17) at location 2 which are critical. These elements overstep the failure criterion at about 75MPa and 65MPa, respectively. For both locations the longitudinal fibers (referred to as *0 ply* in all figures) keep within the failure criterions.

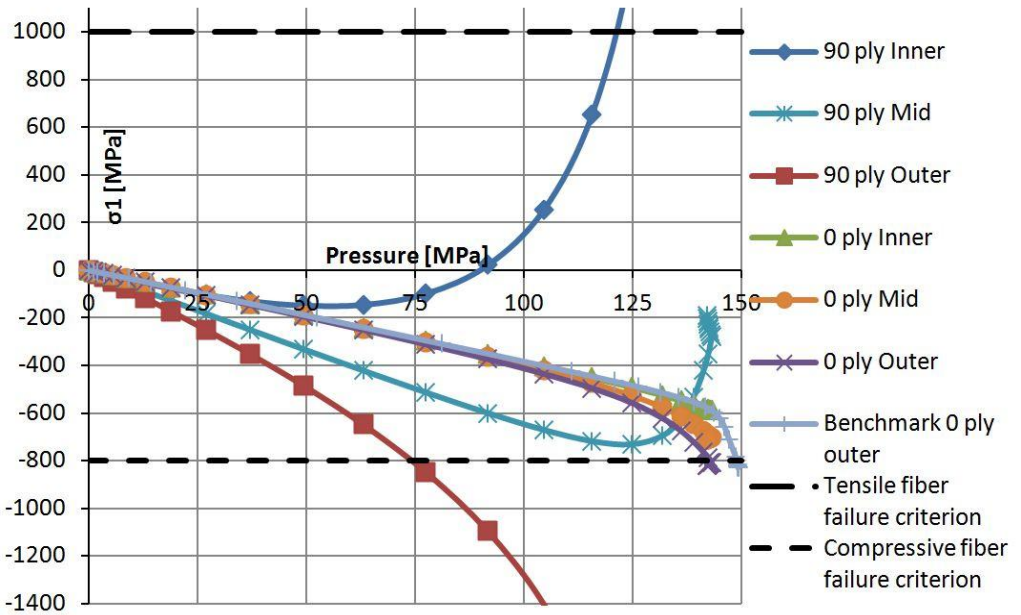
Axisymmetric				RIKS 16 (Location 1)			RIKS 16 (Location 2)		
Element nr	$\sigma_1$ [MPa]	$\sigma_2$ [MPa]	$\sigma_3$ [MPa]	$\sigma_1$ [MPa]	$\sigma_2$ [MPa]	$\sigma_3$ [MPa]	$\sigma_1$ [MPa]	$\sigma_2$ [MPa]	$\sigma_3$ [MPa]
1	-731,5	-32,9	-4,0	253,9	-14,0	0,8	-1838,8	-57,7	-9,0
8	-693,3	-60,0	-54,6	-671,5	-44,4	-23,6	-758,8	-93,2	-109,5
15	-698,3	-83,6	-97,4	-1402,0	-92,5	-86,9	-38,8	-87,4	-122,9
16	-376,6	-98,4	-100,2	-404,3	-139,3	-91,4	-392,0	-67,6	-121,9
23	-376,6	-98,5	-100,1	-420,6	-187,0	-98,2	-374,9	-19,1	-113,4
30	-376,6	-98,6	-100,0	-434,9	-228,0	-104,5	-360,2	21,7	-105,3
Benchmark Outer 0 ply							Benchmark Outer 0 ply		
-387,2							-111,8		
-100,9							-379,8		
							-87,2		
							-101,0		

**Table 10 – Comparing axisymmetric vs. RIKS, D=16mm, P=100MPa, equal thickness of hoop- and longitudinal fibers. Benchmark fields are comparable with values in last row (element nr 30 in axisymmetric model). Lowest element nr is innermost in the structure, and highest element nr is at the outermost location in the structure.**

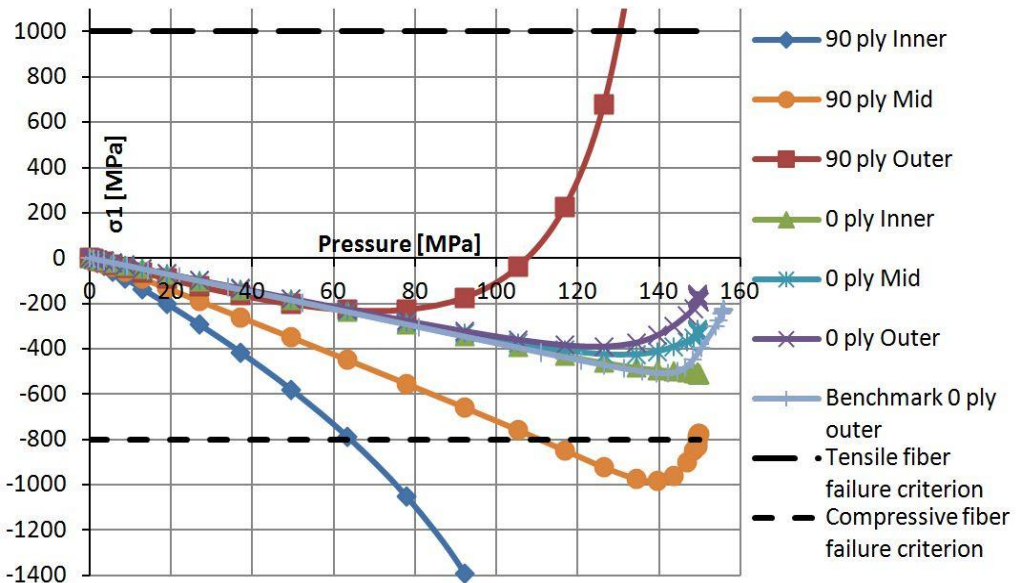
Upon comparison of results from the RIKS analysis with the results from the axisymmetric model, stress values at 100MPa pressure for the six chosen elements in the RIKS model was used. Corresponding elements in the axisymmetric model was used.

Figure 19 show that the maximum pressure ( $S_{33}$  value for outermost element) seems to propagate towards a limit which corresponds to the load factor given by the linear perturbation analysis. In the RIKS analysis the highest pressure value (although after instability has occurred) was 149MPa, for the benchmark it was 155MPa and for the linear perturbation analysis the corresponding load factor was 147 (see Table 9). This is considered to be a very good coherency.

The transverse stress state curves shown in Figure 18 and Figure 19, show that the considered tube dimensions will not fail due to the Puck criterion before instability occurs. This means that the instability which leads to buckling is the governing failure mode for the transverse stress state. Instability, and thus failure, is predicted to about 50MPa.



**Figure 16 - Fiber stresses, development with increasing pressure, D=16mm, Location 1. Compressive fiber failure predicted at about 75MPa pressure. Instability for inner part of hoop ply occurs at about 50MPa pressure.**



**Figure 17 - Fiber stresses, development with increasing pressure, D=16mm, Location 2. Compressive fiber failure predicted at about 65MPa pressure, instability is predicted at about 60MPa pressure.**

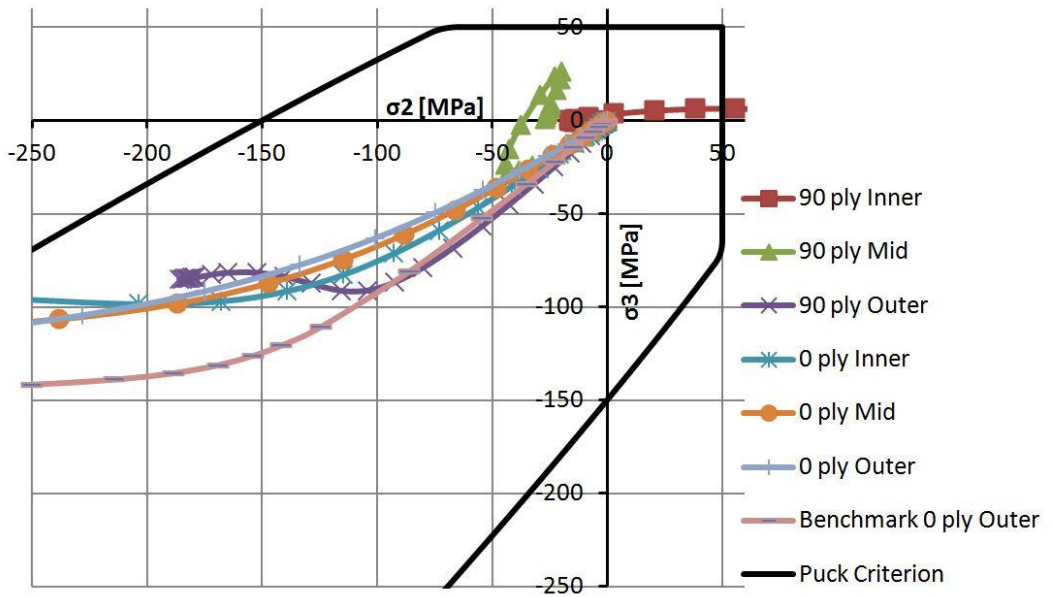


**Figure 18 - Transverse stresses, development with increasing pressure, D=16mm, Location 1. Instability occurs well before Puck criterion predicts failure and predicted to first happen at about 50MPa pressure.**

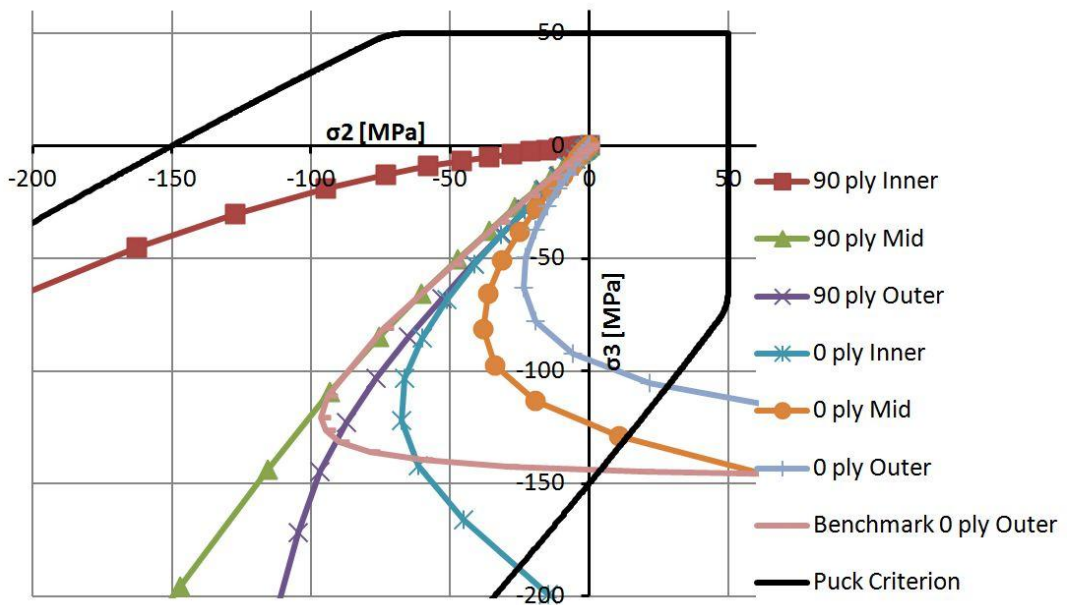


**Figure 19 - Transverse stresses, development with increasing pressure, D=16mm, Location 2. Instability occurs well before Puck criterion predicts failure and predicted to first happen at about 50MPa pressure.**

### 3.3.2 Analysis of 22mm tube

To get results which can both represent the limits given by the requirement specification, and to get scalable results, it was chosen to do an analysis of a D=22mm tube with the same inner diameter as the specimen (d=12mm). This gives a tube with a submerged weight of about 62g/m (see Table 9) including optical fiber, and is on the limit and above regarding both dimensions and weight. However, as the inner diameter is as large as it is, it can be used as a vessel for more than just an optical cable. It was also considered necessary to get results for a really thick-walled structure, as the specimen dimensions (with much thinner walls) cannot be considered relevant dimensions for a final product.

element nr	Axisymmetric			RIKS, Location 1			RIKS, Location 2		
	$\sigma_1$ [MPa]	$\sigma_2$ [MPa]	$\sigma_3$ [MPa]	$\sigma_1$ [MPa]	$\sigma_2$ [MPa]	$\sigma_3$ [MPa]	$\sigma_1$ [MPa]	$\sigma_2$ [MPa]	$\sigma_3$ [MPa]
1	-345,8	-16,8	-3,6	-268,1	-16,8	-5,3	-413,8	-21,4	-8,8
10	-337,8	-45,1	-55,1	-326,3	-40,7	-46,8	-340,6	-47,3	-58,4
20	-418,5	-72,3	-102,1	0,0	-70,0	-96,3	-377,0	-72,0	-102,2
21	-212,8	-82,4	-104,3	-213,0	-83,4	-101,1	-213,6	-80,8	-105,8
30	-212,8	-84,8	-101,9	-214,2	-88,4	-100,1	-212,4	-80,0	-102,6
40	-212,8	-86,7	-100,1	-215,6	-93,7	-99,4	-211,0	-78,4	-99,6

**Table 11 - Comparison, axisymmetric vs. RIKS, D=22mm, P=100MPa, equal thickness of hoop- and longitudinal fibers.**

Between the axisymmetric model and the RIKS model the results are very comparable as instability does not occur until much higher pressures is reached. In general it seems like the axisymmetric model give the average stress of the two locations in the RIKS model. Table 11 also show that stresses are well below the failure criterions at given pressure even when the load factor given by the linear perturbation model was 819 (corresponding to P=8.190 bar, see Table 9).

Comparison of the stress in the 22mm tube in fiber direction (Figure 20 & Figure 21) with the stress in the 16mm tube a significant difference is that through the whole thickness the material stays stable beyond the failure criterion. However, the curves have the same shape and behavior as before. This means that the compressive strength of the fiber is maximally utilized. The first fiber failure is predicted at about 180MPa at location 1 (see *90 ply Outer* line in Figure 20) and at 190MPa at location 2 (see *90 ply Inner* line in Figure 21).

Comparison of the  $\sigma_2$ - $\sigma_3$  curves for the 22mm tube (Figure 22 & Figure 23) with the corresponding curves for the 16mm tube it is quite obvious that the stress development have the same characteristics. What makes the significant difference is at

which pressure the material starts to behave unstable. The curves are staying inside the Puck criterion in both locations, all up to the point of instability. Also here we can observe that the  $\sigma_3$  value for the outermost element (i.e. the pressure) in the structure propagates towards the load factor value found in linear perturbation analysis.

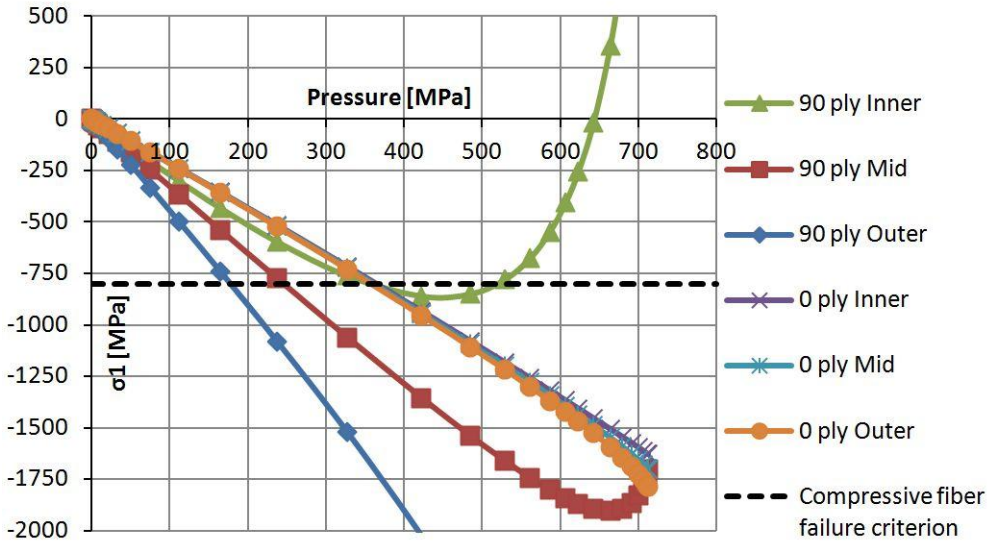


**Figure 20 - Fiber stresses development with increasing pressure, D=22mm, Location 1. No instability before compressive FF occurs (maybe with exception of inner part of hoop ply). Failure predicted at about 180MPa pressure.**

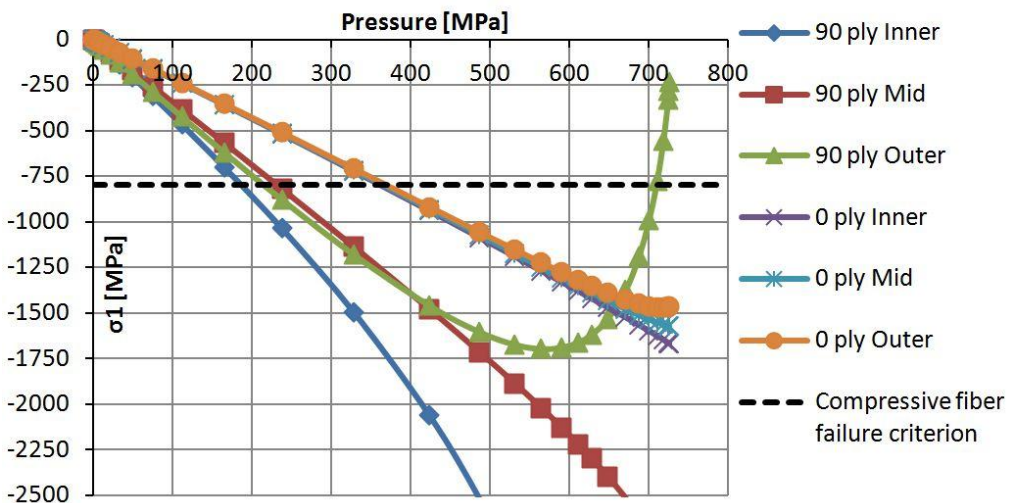


**Figure 21 - Fiber stresses development with increasing pressure, D=22mm, Location 2. No instability before FF criterion predicts failure. Failure predicted at approximately 190 MPa pressure.**



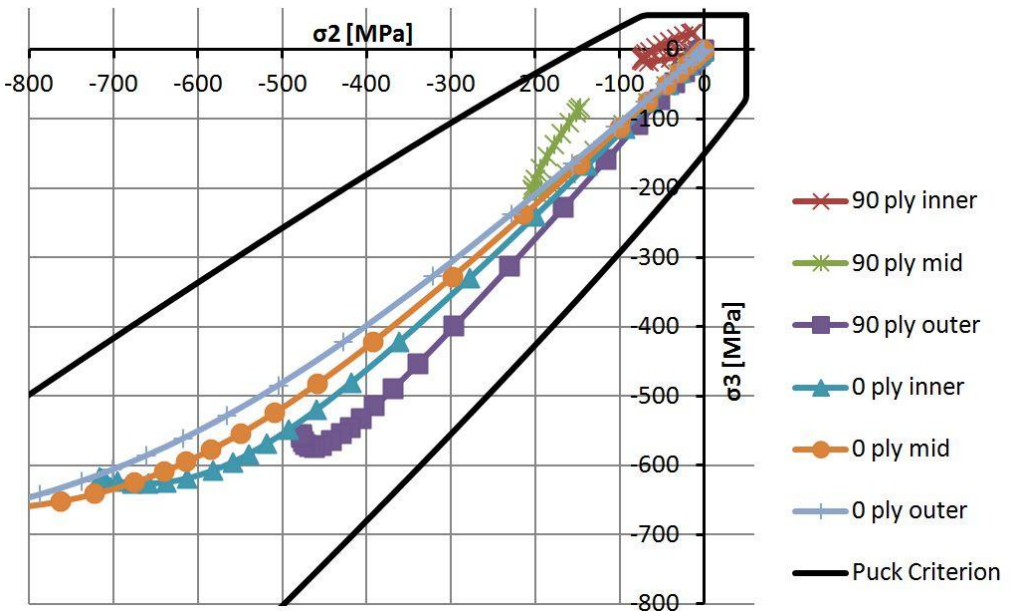


Figure 22 - Transverse stresses, development with increasing pressure, D=22mm, Location 1. Instability will occur at about 420MPa pressure, well before failure predicted by Puck criterion.

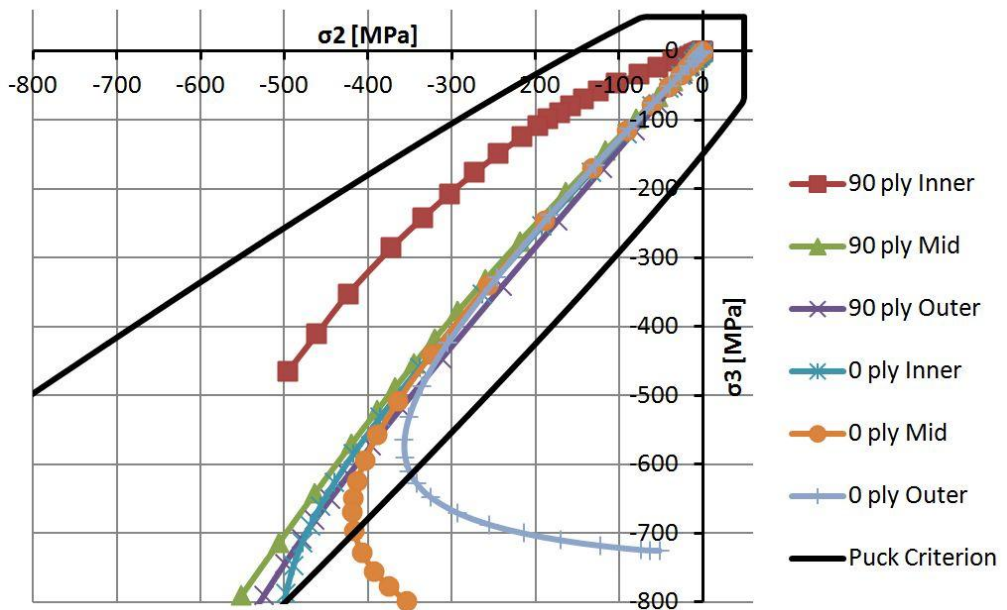


Figure 23 - Transverse stresses, development with increasing pressure, D=22mm, Location 2. Instability will occur at about 530MPa pressure, somewhat before predicted failure by Puck criterion.

### 3.4 Scaling

The dimensions of the 22mm tube can be scaled to more relevant dimensions. The scaling factor, here called  $\lambda$ , has the relation;

$$\begin{aligned} D \cdot \lambda &= D_{new} \\ d \cdot \lambda &= d_{new} \end{aligned} \tag{3.2}$$

where  $d$  and  $D$  represents the inner and outer diameter, respectively.

By scaling in this way you will obtain the same results for any dimension. This is only true if also mesh element size is scaled with the same factor, and load and boundary conditions stay unchanged. A benchmark to see if this is correct for the linear perturbation model was made with  $\lambda=0,5$  and the load factor given was the same as if  $\lambda=1$ .

The same test was done with the RIKS model.  $\lambda=0,5$  was used, also for the geometric imperfection. Results from this analysis also looked the same, but the arc length steps were different, so 100% certain it is not. Since the elements are manually picked for each analysis the variation could be because a nearby element was picked in the benchmark instead of the same as before. However, the difference found was so small that it is negligible. All stress curves for the RIKS analysis of the 11mm scaled tube is given in Appendix 3.

Notice is that by scaling the diameters like this the submerged weight change (for this particular case with  $d=12\text{mm}$ ,  $D=22\text{mm}$  and  $\lambda < 1$  the submerged weight will decrease). This is very usable in the sense that an analysis of a specific tube can be scaled to the desired weight.

$\lambda$	D [mm]	d [mm]	Sub, weight with fiber optics [g/m]
1	22	12	62,1
0,9	19,8	10,8	53,2
0,8	17,6	9,6	45,2
0,7	15,4	8,4	38,1
0,6	13,2	7,2	32,0
0,5	11	6	26,8

**Table 12 - Weights of scaled tube with original dimensions  $D=22\text{mm}$  and  $d=12\text{mm}$ .**

## 4 Experimental

Specimens were made with a layup of equal thickness of hoop and longitudinal fibers as described in section 1.4, with the corresponding dimensions to previous analysis. These specimens were sent to the University of Aberdeen for testing.

### 4.1 Production of specimens

The inner diameter for the tube, meaning the diameter of the mandrel, was chosen to be 12mm. This dimension was chosen both to enable removal of the mandrel after the winding process, and so that the needed test pressure for buckling/failure would not exceed 1000bar as accurate test equipment delivering considerable higher pressures were not available at the production stage (test equipment had an upper limit capacity of 2000bar). Another factor was that the shortest mandrel possible in the filament winding machine, without having an unsupported end, was just below 1m. The implication would be that the force from the fiber when winding could cause a thin mandrel to deflect.

Steel mandrel, 12mm solid rod	S355J2G3C+C+SL, ISO286 H6, grinded surface
Fiber	AS7 ( $E_f = 238\text{GPa}$ )
Release agent	Chemlease® 5151 FLANGE WAX
Resin base	EPICOTE™ Resin MGS RIMR 135
Resin cure	EPIKURE™ Curing Agent MGS RIMH 137

**Table 13 - Data on components used to make specimens**

Mandrel lengths of 1m were used in the filament winding process making the layer of hoop fibers. Before winding the fiber a release agent was added to the surface of the mandrel. During the winding process the fiber was winded on to the mandrel in dry state and the resin was added with a brush between each layer. The fiber was laid on with an angle of  $\pm 88,5^\circ$ . This method leaves high uncertainty related to volume fraction of fiber and could be a source of error.

After the hoop fibers was laid winded, and the resin had hardened in room temperature, excess composite material was removed using a turning machining process and the specified outer diameter of 14mm was obtained. To see accurate final dimensions see Appendix 2.

#### 4.1.1 Production of longitudinal fiber layer

To get longitudinal fibers on the specimens, two different approaches were tried. Both consisted of first winding fiber onto a 10cm diameter mandrel in sufficient thickness. Then the fiber was cut and pulled off in a single sheet while still wet.

Approach 1: The sheet was rolled onto the specimen with a peel ply around and the peel ply was at last tightened and clamped, before left to cure in room temperature overnight.

Approach 2: The sheet was rolled onto a specimen, and peel ply was added on top. The specimen was then placed into a mold consisting of two halves of a tube. Two clamps were tightened around the mold, evicting superfluous resin.

Approach 2 was worked out because of very uneven finish regarding circularity of approach 1, and all specimens was made with approach 2 with exception of one. Both methods leaves uncertainty to volume fraction of fiber, but it is reasonable to believe approach 2 will give the highest fraction and the best distribution.



**Figure 24 – The moulds used for specimen production using approach 2. The holes in the mold facilitate escaping of superfluous resin.**

Due to the manual impregnation of fibers voids were expected the manual molding was expected to give an uneven distribution of fibers with large local variations. The production method was thus expected to give a large scatter in the test results.

#### **4.1.2 Completing specimen**

After curing in room temperature for about 18 hours the specimens was released from their mold and peel ply. Specimen from approach 1 was machined down to about 18mm in outer diameter. The machining took place before curing because of the severe oval form caused by the free hand layup; the concern was that a hardened specimen might crack and disintegrate if cured before machining. All specimens were cured in oven for 6 hours at 80°C, before final machining to 16mm outer diameter and desired length. See Appendix 2 for details around final geometric sizes and curing data for each specimen.

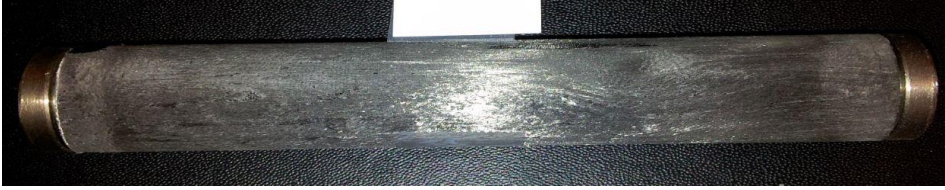


**Figure 25 - Finished specimen with end caps. Silicon is not added on surface yet.**

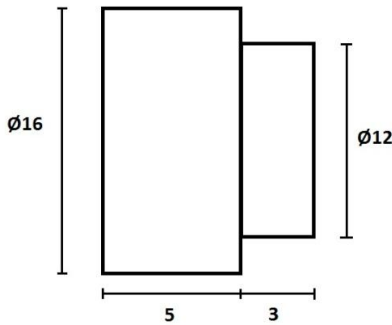


**Figure 26 - End cap dimensions (all dimensions in [mm])**

The end caps were machined out of steel with dimensions as shown in Figure 26. When assembling end caps to the composite tube silicon was as bonding agent. Silicon was chosen due its high elasticity and sealing qualities. After sealing the ends the whole outer surface of the tubes were covered with a thin layer of silicon to prevent any leakage through the material. The silicon is considered to add neither stiffness nor strength to the structure.

A total of 8 specimens were made, but only 5 of these were sent for testing. This was due to the length of the specimens. Only in 4 of the specimens the final length became 120mm. It was desired to have equal lengths on all specimens. The last specimen sent for testing was shorter, but the reason for this was to have the opportunity to do a trial test before testing the 4 specimens with equal length.

#### **4.1.3 Estimated elastic properties of specimens**

Important for the elastic properties is the volume fraction of fibers. This parameter can be estimated from images of a section of the material, by comparing the area of fibers versus the total area.

According to composite theory the final elastic modulus will yield the Rule of Mixture.

$$E_1 = V_f E_f + (1 - V_f) E_m \quad (4.1)$$

where  $E_m$  is the elastic modulus of the matrix, assumed to be 2GPa, and  $V_f$  represent the volume fraction of fibers.

Section images of two specimens were used to estimate the volume fraction. The specimens used were specimen nr2 and nr8. As the volume fraction in the longitudinal layer of specimen nr8 is predicted to be lower than for the other specimens, only pictures of the hoop layer was taken of this specimen. As the volume fraction in the hoop fibers for all specimens is assumed to be similar, only pictures of longitudinal fibers were taken of specimen nr2.

#### 4.1.3.1 Volume fraction of hoop fibers

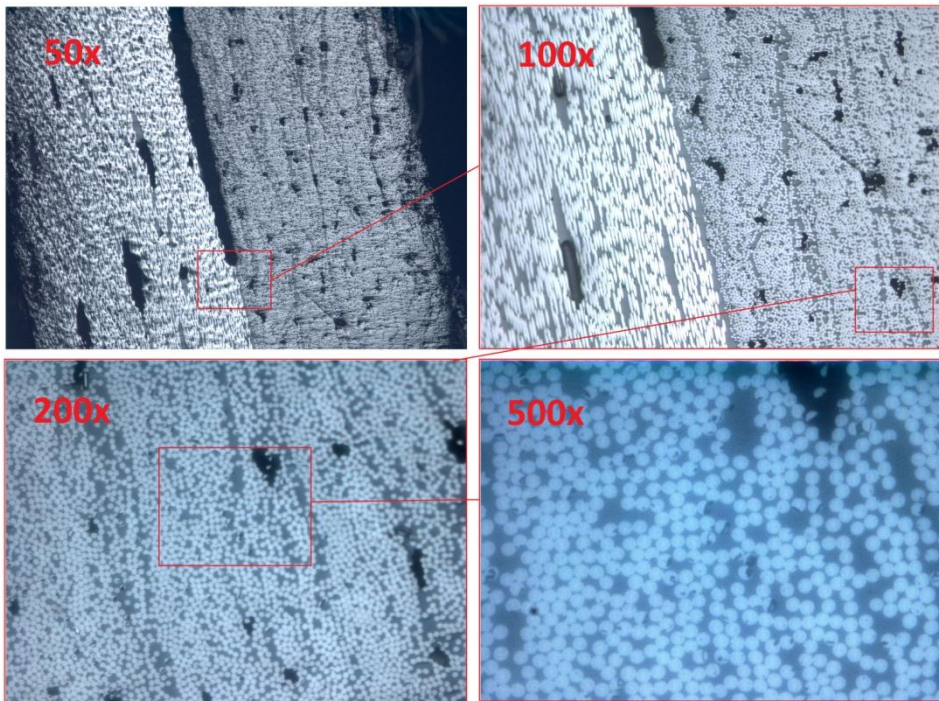


**Figure 27 – Microscopy of specimen nr8, zooming in on the hoop fibers (enhancement is indicated in top left corner of each image). This is the original images before rendering. The large crack between the hoop and longitudinal layer in the top left image is believed to be a result of the machining process.**

To analyze the images the freeware *ImageJ* [8] was used. The method used to estimate the volume fraction was to estimate the total area of fibers. First step is to render the images; first transformation to grayscale and tweak the contrast to make the fibers as clear as possible.

Figure 28 and Figure 29 show rendered versions of the 500x zoom image in Figure 27. Due to issues with contrast in the images the top and left edge of the images became



too dark after rendering. The approach therefore was to use two different levels of contrast; one considered to be a relatively conservative estimate of fibers, and one giving a relatively high estimate of fibers.

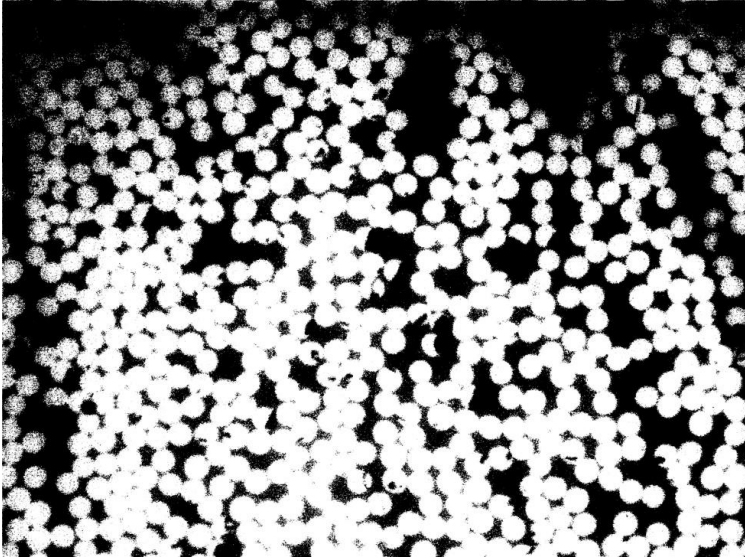


**Figure 28 – Rendered image of hoop fiber layer in specimen nr8, with 500x enhancement. The volume fraction calculated is considered to be somewhat conservative due to the dark edges. Estimated volume fraction: 0,526.**

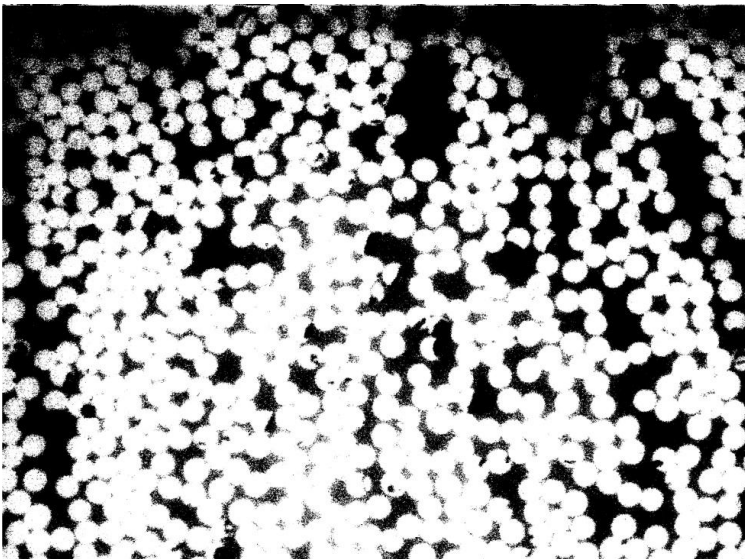


**Figure 29 – Rendered image of hoop fiber layer in specimen nr8, with 500x enhancement. The volume fraction calculated is considered to be somewhat high as space between fibers from parts of picture is quite bright. Estimated volume fraction: 0,596.**

In addition to the two images showed in Figure 28 and Figure 29, which shows the same part of a section, additional images of other parts of the same section was used to estimate the volume fraction (images presented in Appendix 4) using the same approach (one giving a conservative estimate and one giving a high estimate) as described earlier in this section. The average volume fraction estimated by a total of 6 images was 0,564. The rule of mixture then give an estimated elastic modulus  $E_1=135,1\text{GPa}$ .

#### 4.1.3.2 Volume fraction of longitudinal fibers

As estimating the volume fraction for the longitudinal fiber layer was not considered important compared to the hoop layer, a slightly different approach was used. A total of 4 images with enhancement 50x, 100x, 200x and 500x was used. The effect of dark edges seemed to be most critical for the highest enhancement. The remaining 3 images was therefore assumed to be accurate enough without using the same approach as for the hoop fiber section.

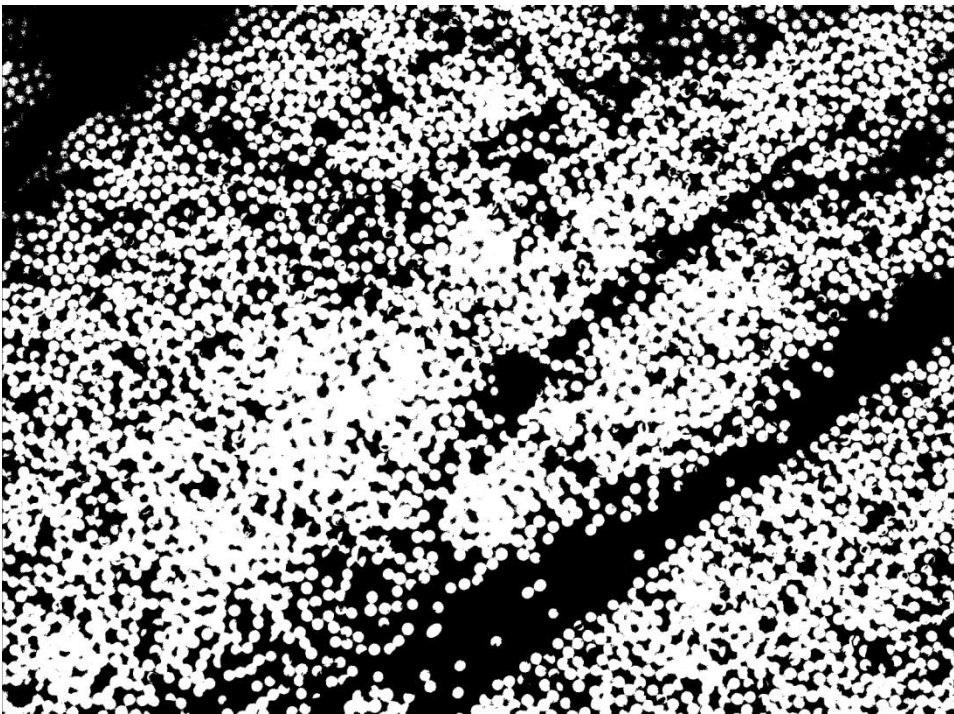


**Figure 30 – Rendered image of hoop fiber layer in specimen nr2, with 200x enhancement. Estimated volume fraction: 0,527.**

Average estimated volume fraction in longitudinal fiber layer was 0,537, slightly lower than the estimate for hoop layer. The elastic modulus for the longitudinal layer was



calculated to  $E_1=128,7\text{GPa}$ . The additional 3 images used for the estimate is presented in Appendix 5.

Microscopy unveiled moderate to large voids in the structure as assumed by the production method, strengthening the assumption of large scatter in test results.

## 4.2 Test procedure

Out of the 5 samples sent for testing one specimen was shorter than the others (nr.4). This specimen was used to check if the test equipment worked properly. The test procedure for this specimen was to increase the pressure in steps of 5MPa and holding it some time for each step, until failure occurred.

The remaining four samples had a slightly different test procedure. Here the pressure increased linearly to 70MPa over about 2 minutes. If the sample had not failed the pressure was increased in steps of 5MPa until failure occurred.

No other measurement than the pressure were logged during the testing. Pressure was logged every 1 second interval. Upon failure a loud bang was heard and the pressure dropped with 2MPa.

## 4.3 Test results

The pressure at which failure occurred had a quite large scatter. The lowest critical pressure was 53MPa and the highest was 105MPa.

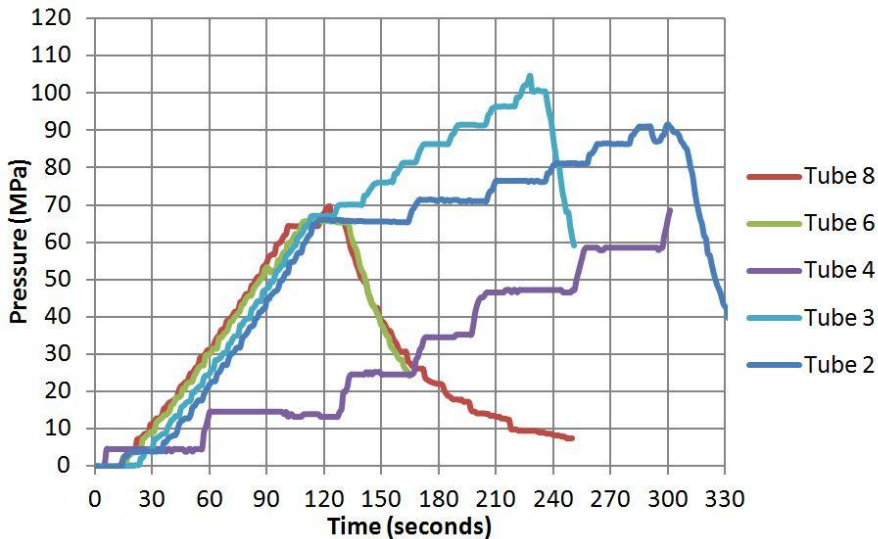


**Figure 31 – Recorded pressure vs. time during testing for all specimens. The large decrease in pressure shown for some specimens represents the depressurization of the pressure chamber.**

Specimen nr.	2	3	4	6	8
Failing pressure [MPa]	91	105	70	53	69

**Table 14 – Critical pressure for all specimens**

The results have a large range in critical pressure. The 53MPa obtained with specimen nr.6 is about what was expected as worst case scenario when compared to the RIKS analysis which predicted instability (and thus failure) at about 50MPa (see Figure 18 and Figure 19). If it would be possible to make a perfect tube with perfect fiber orientation the predicted critical pressure from the analysis was 148MPa (see Table 9), and the highest critical pressure recorded, obtained with specimen nr.3, is about two thirds of this. It can be concluded that all tests are within the predicted range of which failure occurs.

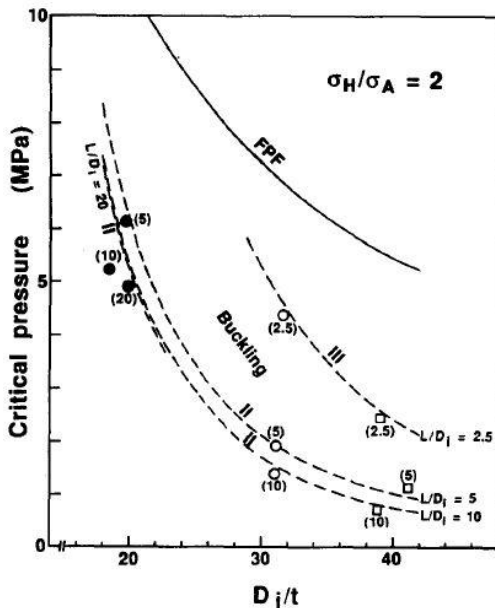


**Fig. 6.** Plot of critical pressure versus  $D_i/t$  for samples tested at a stress ratio  $\sigma_h/\sigma_a=2$ .  $L/D_i$  values are shown adjacent to experimental points. (---) Computed buckling pressures for various sample aspect ratios and wave numbers (I, II); (—) FPF) computed first-ply failure pressures.

**Figure 32 – Relations between critical pressure and inner diameter to thickness ratio for different length to inner diameter ratios. Hoop to longitudinal stress ratio is 2. (Failure of composite cylinders under combined external pressure and axial loading, 1992 [5])**

Mistry [5] found a relation between critical pressure versus inner diameter to thickness ratio ( $D_i/t$ ) for various length to inner diameter ratios ( $L/D_i$ ). Figure 32 shows the mentioned relation when hoop to axial stress ratio equals 2.

The tested specimens had a hoop to axial stress ratio of 2 and a  $L/D_i$  ratio of 10. However, the figure only shows the relation in a range from 0MPa to 10MPa, far below the critical pressure found for the specimens. Mistry also used a different orientation in his layup than used in this thesis, and all together the specimens can not be compared to Mistry's work. However, the figure show a trend when the  $D_i/t$  ratio declines the critical pressure increase exponentially, which is in keeping with the specimen results. Axial stress in this context refers to average stress in the axial direction.



**Figure 33 - Specimen 2 after failure. Critical pressure = 91MPa.**



**Figure 34 - Specimen 3 after failure. Critical pressure = 105MPa.**



**Figure 35 - Specimen 4 after failure. Critical pressure = 70MPa.**



**Figure 36 - Specimen 6 after failure. Critical pressure = 53MPa.**



**Figure 37 - Specimen 8 after failure. Critical pressure = 69MPa.**

The failed specimens showed severe damage along the whole length, both in the hoop layer and the longitudinal layer. Ovaling of the tube (with following collapse) was assumed as failure mode. Figure 33 to Figure 37, shows the failed specimens. The tubes have been split in half along the length. Specimen 8 is so damaged that this conclusion may not be consistent for this particular specimen, but the part in the left of the image clearly shows such a split. This indicates coherency with the assumed failure mode.

## 5 Discussion

Both the linear perturbation and the RIKS model have assumptions concerning the geometry which represent a source of error. The linear perturbation model assumes that both material and geometry of the tube is perfectly circular, which leads to a result giving the absolute maximum pressure before failure, but this pressure will in reality be impossible to obtain. In the RIKS model there is introduced an imperfection to the geometry, in this case a slightly elliptic shape. This imperfection is hard to estimate correctly. The introduced imperfection is the soul parameter governing at which point instability occurs. The RIKS model predicts the same maximum pressure as the linear perturbation model, if the imperfection converges towards zero. However, this assumption is completely unrealistic for such a rod, especially since even small imperfections will be relatively large compared to the overall dimensions.

The size of the imperfection used in the RIKS analysis was intended to simulate a worst case scenario. Since the linear perturbation model has perfect geometry, the results from this model could be considered as best case scenario. Results from specimen tests were therefore predicted to be in the range between these two extremes.

It was predicted a quite large scatter in pressure at which the specimens failed, and it can be explained with the manual production process. Neither manual impregnation (with a brush) of the fibers, machining the specimens nor manual “moulding” of longitudinal fibers are even close to being optimal methods, and the total of the whole process gives low control over the quality of each specimen. Local differences inside the material, especially voids which locally lowers the strength a great deal, and local density of fibers which inflict on the properties of the composite. When a proper (industrial) production process is set up the composite quality surely will be better.

Some of the variation in the failure pressure between the specimens could be explained with variation in elastic modulus. The elastic modulus determines how the stress is distributed in the structure and the modulus is governed by the volume fraction of fibers. Variations in the volume fractions in this case are a result of the manual production process. Images taken to estimate this value was only taken from two of the specimens. In one specimen images was taken of the hoop fibers and in the other the longitudinal fibers. Variations in the fiber volume fractions were assumed to be negligible, but no quantifiable data was gathered. Estimated elastic modulus was also somewhat lower than the one used in the analysis, but as the test results vary as much as they do this difference is negligible in the set context.

Assuming that there were differences regarding the quality of the structure, the differences in damage on each specimen can also be explained. As specimens with the most imperfections in the structure would then not only obtain the lowest critical

pressure, but also fail in the most inconsistent and dramatic way. From Figure 33 to Figure 37 it is clearly seen that the two specimens with the most damage is the two which obtained the lowest critical pressure.

Analysis performed with specimen dimensions predicted failure as a result of instability at about 50MPa, representing worst case scenario. Corresponding failure pressure in best case scenario was predicted to be 148MPa. All test results from specimens lie in between these two values. It also seems that the assumed failure mode was correct.

## **5.1 Future work**

The next step in analysis is to look at how the stresses evolve when the tube in addition to the pressure and longitudinal force is subjected to bending. This is necessary as this will probably decrease the critical pressure. Since the tube will have to go around bends in the well this load case is highly realistic.

A challenging task will be to get accurate test results for tubes with usable dimensions. This implies that pressure equipment which can withstand considerable higher pressures must be utilized. Tests with higher quality specimens and several specimens could be conducted to achieve statistic significance.

Strains in the material and failure strain criterions have not been subject in this thesis and should be considered in future work.

Also not subject in this thesis have been the effects of creep. As the tube is going to be stored on a drum for a considerable amount of time between each use, investigations on creep should be taken on.

Even though carbon composites do not have large issues with fatigue it should be investigated as the magnitude of the loads are considerable. No work on the subject of fatigue has been conducted for this rod as no data load conditions for such a case were available (well conditions).

The analyses conducted in this thesis only corresponds to how the tube is loaded when it has been submerged in the well, not moving, with no bending effects, which means that the longitudinal force corresponds to the force generated by the pressure only. Analysis with larger, or smaller, longitudinal force relatively to the pressure the curves are believed to shift as explained in Figure 14. This could lead to failure according to Pucks criterion before instability occurs. This is highly relevant as insertion and withdrawing the tube will generate such load cases.

## 6 Conclusion

The objective of this thesis was to conduct a feasibility study on thick walled tubes subjected to high pressures, for use in oil wells. Both analytical and experimental work has been used to answer questions around this topic.

Analysis show that under given loading conditions the chosen structure fails due to material instability. This means that the material strength capacity is maximally utilized.

Results from experimental work are in keeping with the predicted failure mode and critical pressure. Test results are coherent with analyses but have a large scatter and thus lack statistic significance. The scatter is explained by the production method leading to high variation in local material properties due to voids and fiber density.

Experimental work was funded in analysis of tube dimensions which can not be considered realistic for the intended use. They are however representative concerning stress propagation. Analysis on larger dimensions, which could be considered for the final product, has been carried out and a method of scaling dimensions without inflicting stress propagation has been identified.

The layup used in analysis and experimental work was, out of all considered possibilities, assumed to be the best alternative to satisfy the requirements given. Although no work on optimizing the layup has been conducted, results from both analytical and experimental work are promising.

More work is needed on several topics which were considered out of scope in this thesis, such as temperature requirements. However, there are no indications based in this work which would lead to the conclusion that a carbon composite tube would not be possible to use for high pressure applications.

## 7 References

1. Dong, L. and J. Mistry, *An experimental study of the failure of composite cylinders subjected to combined external pressure and axial compression*. Composite Structures, 1997. **40**(1): p. 81-94.
2. Ouellette, P., S.V. Hoa, and T.S. Sankar, *BUCKLING OF COMPOSITE CYLINDERS UNDER EXTERNAL PRESSURE*. Polymer Composites, 1986. **7**(5): p. 363-374.
3. Hernández-Moreno, H., et al., *Influence of winding pattern on the mechanical behavior of filament wound composite cylinders under external pressure*. Composites Science and Technology, 2008. **68**(3-4): p. 1015-1024.
4. Moon, C.-J., et al., *Buckling of filament-wound composite cylinders subjected to hydrostatic pressure for underwater vehicle applications*. Composite Structures, 2010. **92**(9): p. 2241-2251.
5. Mistry, J., A.G. Gibson, and Y.S. Wu, *Failure of composite cylinders under combined external pressure and axial loading*. Composite Structures, 1992. **22**(4): p. 193-200.
6. Knops, M., *Analysis of failure in fiber polymer laminates : the theory of Alfred Puck*2008, Heidelberg ; New York: Springer. xi, 205 p.
7. *Abaqus 6.10 Documentation*, 2010, Dassault Systèmes Simulia Corp.
8. Health, U.N.I.o.; Available from: <http://rsbweb.nih.gov/ij/index.html>.



## Appendix 1

Longitudinal and bending stiffness for tubes with 60% longitudinal and 40% hoop fibers  
(Layup model 2 in Figure 3)

D [mm]	Submerged weight with fibreoptics [g/m]	Longitudinal Stiffness, $K=A^*E$ [MPa]	Bending stiffness [MPa*mm <sup>4</sup> ]
14	0,07	8,14E+06	1,61E+08
15	0,34	9,50E+06	2,15E+08
16	0,50	1,10E+07	2,81E+08
17	0,24	1,25E+07	3,61E+08
18	0,04	1,41E+07	4,56E+08
19	0,22	1,58E+07	5,70E+08
20	0,81	1,77E+07	7,04E+08
21	0,53	1,96E+07	8,58E+08
22	0,28	2,15E+07	1,04E+09

**Table 15 - Longitudinal and bending stiffness for 0 g/m tubes with layup model 2.**

D [mm]	Submerged weight with fibreoptics [g/m]	Longitudinal Stiffness, $K=A^*E$ [MPa]	Bending stiffness [MPa*mm <sup>4</sup> ]
14	49,26	1,15E+07	2,06E+08
15	50,34	1,30E+07	2,68E+08
16	49,07	1,43E+07	3,40E+08
17	49,40	1,58E+07	4,28E+08
18	49,44	1,75E+07	5,32E+08
19	49,20	1,92E+07	6,53E+08
20	51,44	2,11E+07	7,99E+08
21	50,80	2,30E+07	9,63E+08
22	49,86	2,49E+07	1,15E+09

**Table 16 - Longitudinal and bending stiffness for 50 g/m tubes with layup model 2.**

## Appendix 2

Data on all specimens made. Specimen numbers marked with green are specimens sent for testing in pressure chamber.

Specimen nr 8 which is marked in red is the one specimen which was made with approach 1. Measurements were done with a slide caliper which had a precision of 0,05mm.

	Specimen	1	2	3	4	
Diameter on Hoop Layer, After Machining	Max [mm]	14,10	14,00	14,10	14,00	14,10
	Min [mm]	13,95	13,95	14,00	13,90	14,00
	Average	14,03	13,98	14,05	13,95	14,00
	Spread	0,15	0,05	0,10	0,10	0,15
Diameter on Longitudinal Layer, After Machining	Max [mm]	16,10	16,15	16,05	16,05	16,05
	Min [mm]	16,05	16,10	16,00	16,00	15,95
	Average	16,08	16,13	16,03	16,03	16,00
	Spread	0,05	0,05	0,05	0,05	0,10
Length [mm]		109,8	120,2	119,75	98,3	114,0
L/Di		9,15	10,02	9,98	8,19	9,50
Curing	Drying time (before curing) time [hours]	17,5	40	16	16	17,5
	time [hours]	6	7	6	6	6
	max Temperature (°C)	82,5	80	85	85	82,5

Table 17 - Specimen data

### Appendix 3

Stress curves from RIKS analysis on 11mm scaled tube (scaled from 22mm tube with inner diameter of 12mm).

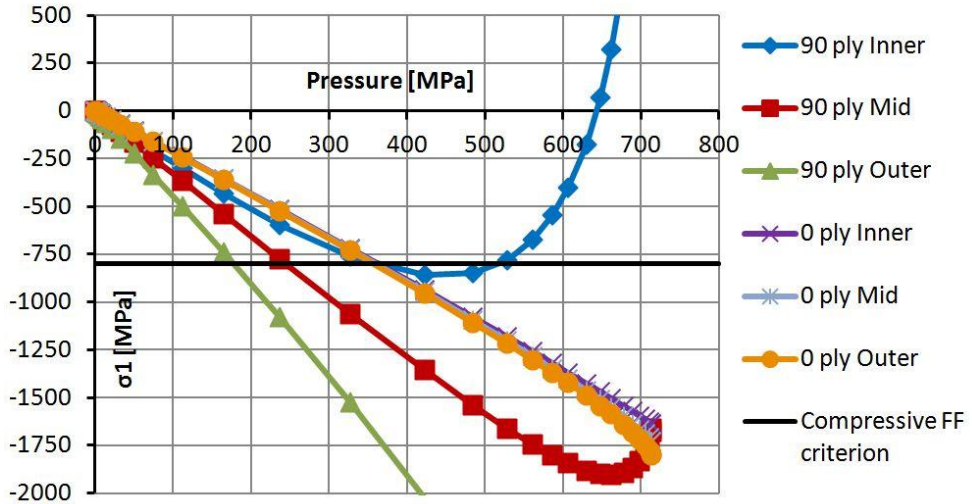


Figure 38 - Fiber stresses, development with increasing pressure, D=11mm, Location 1. Compressive fiber failure predicted at about 180MPa pressure, occurring before instability.

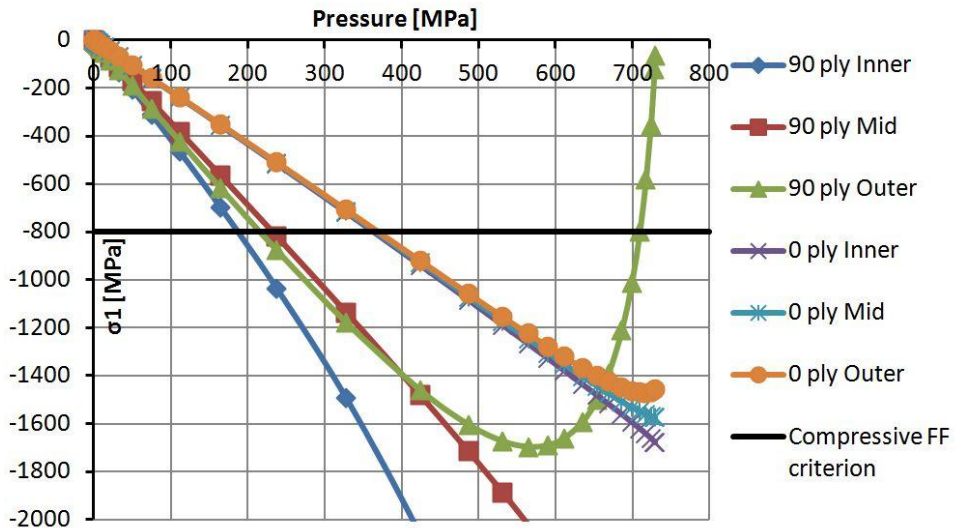


Figure 39 - Fiber stresses, development with increasing pressure, D=11mm, Location 2. Compressive fiber failure predicted at about 190MPa pressure, occurring before instability.

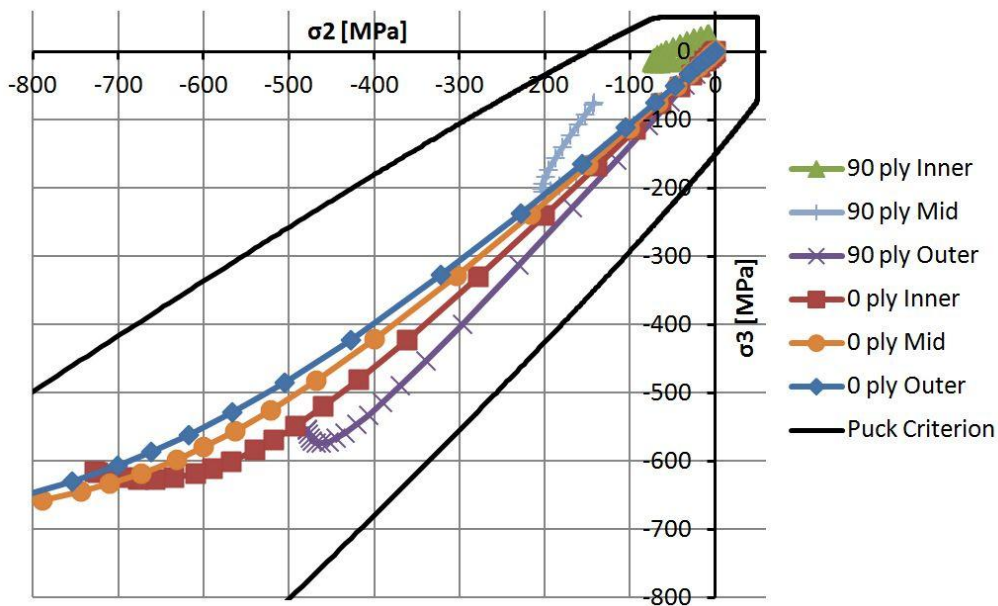


Figure 40 - Transverse stresses, development with increasing pressure, D=11mm, Location 1. Instability predicted at about 420MPa pressure, before Puck criterion predicts failure.

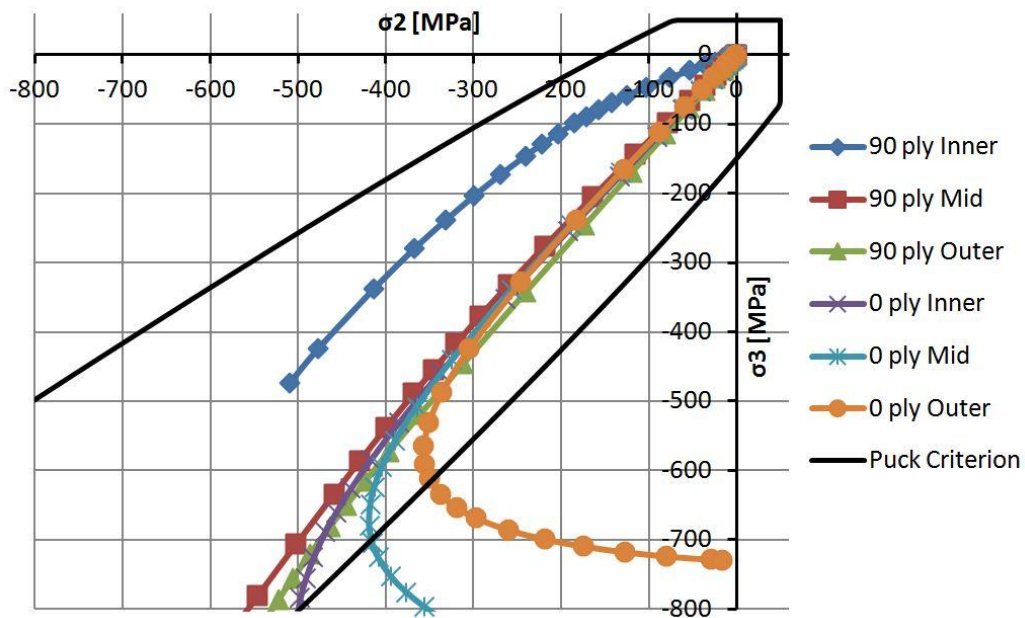


Figure 41 - Transverse stresses, development with increasing pressure, D=11mm, Location 2. Instability predicted at about 530MPa pressure, before Puck criterion predicts failure.

## Appendix 4

Here the 5 images, in addition to Figure 28 and Figure 29, used for estimating the elastic modulus of the hoop layer in the specimens presented.

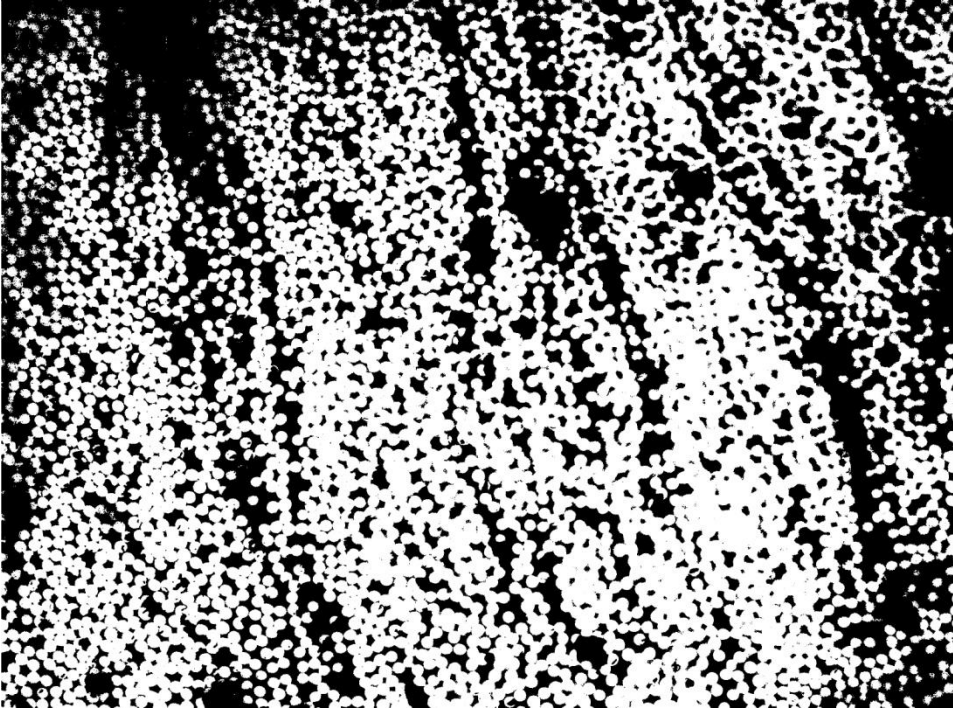
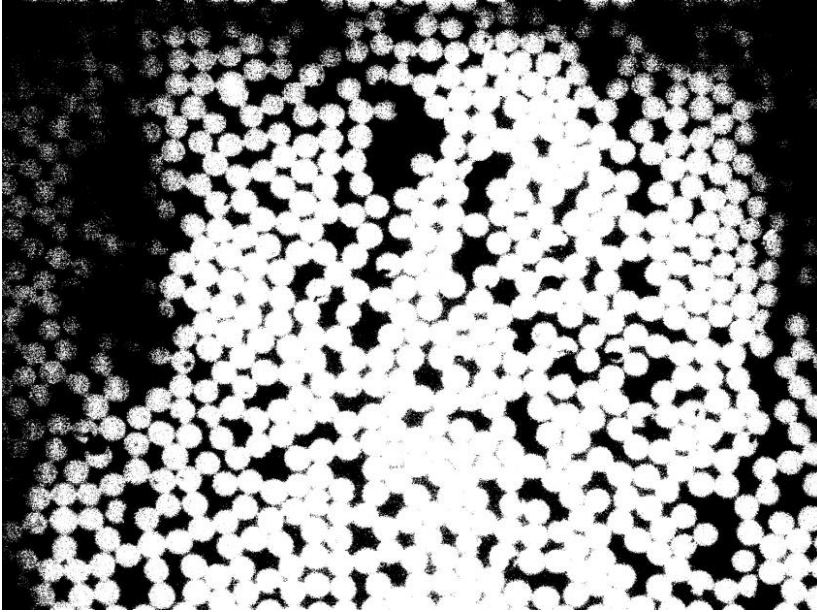
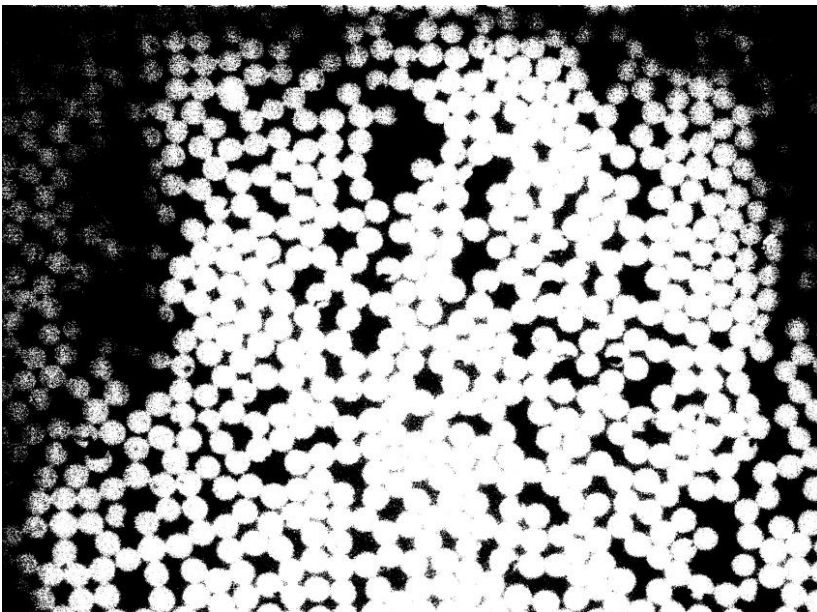


Figure 42 – Rendered image of hoop fiber layer in specimen nr8, with 200x enhancement. Estimated volume fraction: 0,554.



**Figure 43 – Rendered image of hoop fiber layer in specimen nr8, with 500x enhancement. The volume fraction calculated is considered to be somewhat conservative due to the dark edges. Second part of the used section. Estimated volume fraction: 0,543.**



**Figure 44 – Rendered image of hoop fiber layer in specimen nr8, with 500x enhancement. The volume fraction calculated is considered to be somewhat high as space between fibers from parts of picture is quite bright. Second part of the used section. Estimated volume fraction: 0,623.**

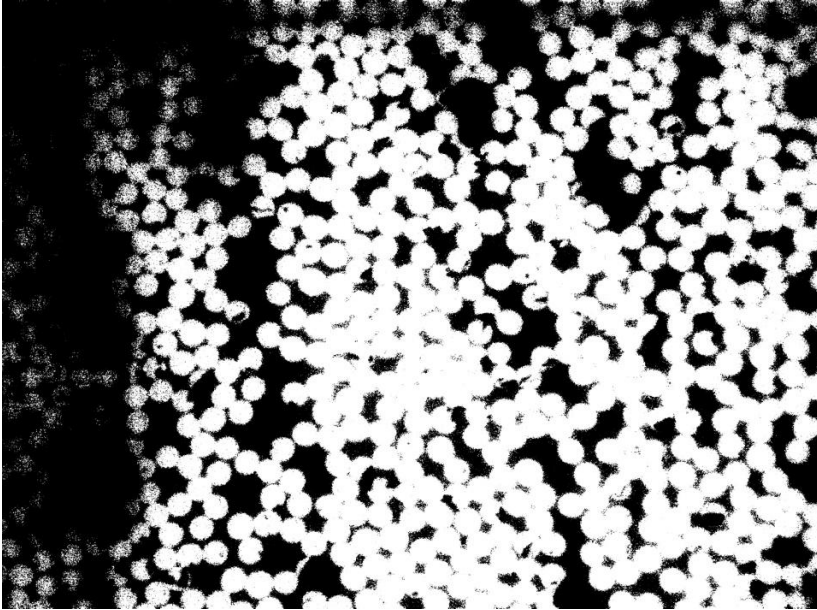


**Figure 45 – Rendered image of hoop fiber layer in specimen nr8, with 500x enhancement. The volume fraction calculated is considered to be somewhat conservative due to the dark edges. Second part of the used section. Estimated volume fraction: 0,508.**

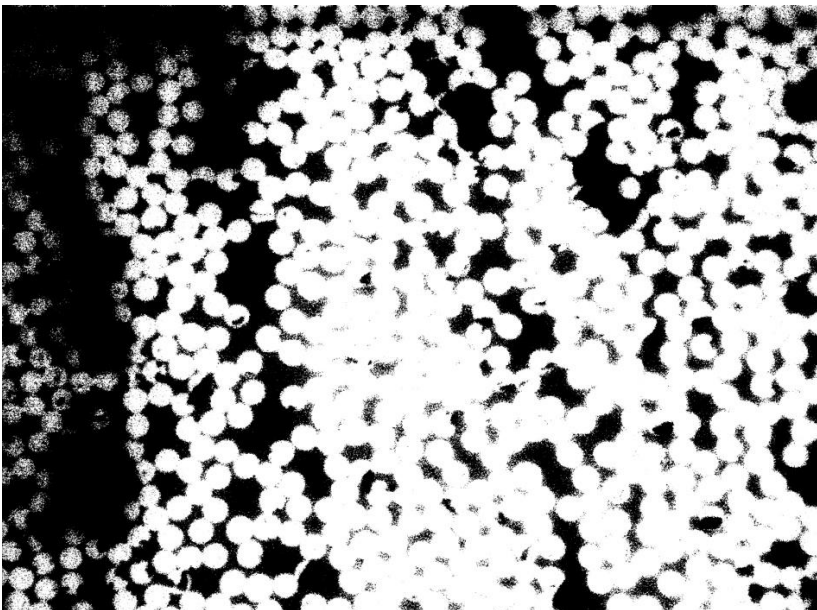


**Figure 46 – Rendered image of hoop fiber layer in specimen nr8, with 500x enhancement. The volume fraction calculated is considered to be somewhat high as space between fibers from parts of picture is quite bright. Second part of the used section. Estimated volume fraction: 0,596.**



## Appendix 5

Here the three images, in addition to Figure 30, is presented.

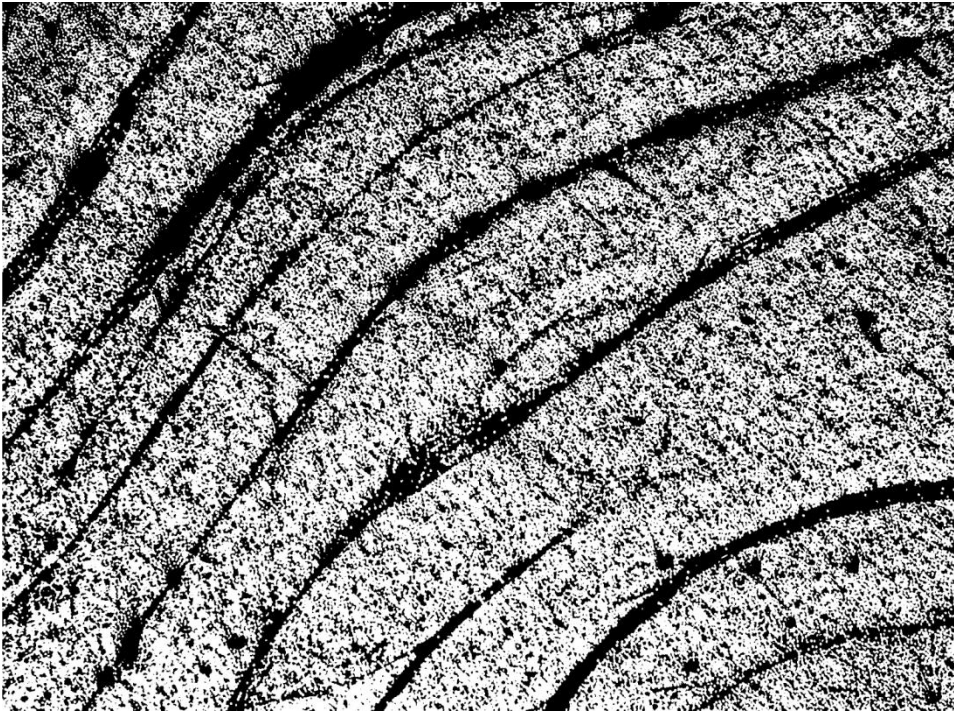


Figure 47 – Rendered image of hoop fiber layer in specimen nr2, with 50x enhancement. Estimated volume fraction: 0,534.





Figure 48 – Rendered image of hoop fiber layer in specimen nr2, with 100x enhancement. Estimated volume fraction: 0,558.

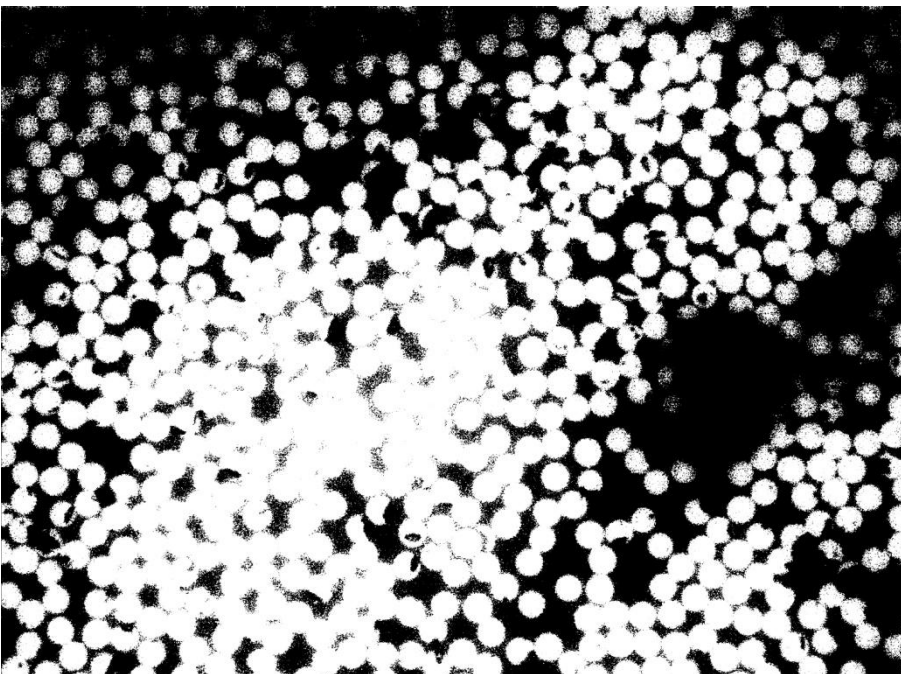


Figure 49 – Rendered image of hoop fiber layer in specimen nr2, with 500x enhancement. Estimated volume fraction: 0,530.